A SIMPLIFIED TECHNIQUE FOR PHASE CONTROL OF CONFORMAL ARRAYS

J. B. L. Rao, et al

Naval Research Laboratory
Washington, D. C.

10 March 1975

SECURITY CLASSIFICATION OF THIS PAGE *(When Data Entered)*

REPORT DOCUMENTATION PAGE

READ INSTRUCTIONS BEFORE COMPLETING FORM

1. REPORT NUMBER: NRL Report 7856	2. GOVT ACCESSION NO.
3. RECIPIENT'S CATALOG NUMBER: AD/A007 436	
4. TITLE *(and Subtitle)*: A SIMPLIFIED TECHNIQUE FOR PHASE CONTROL OF CONFORMAL ARRAYS	5. TYPE OF REPORT & PERIOD COVERED: Interim report on a continuing NRL problem
	6. PERFORMING ORG. REPORT NUMBER
7. AUTHOR(s): J.B.L. Rao and J.K. Hsiao	8. CONTRACT OR GRANT NUMBER(s)
9. PERFORMING ORGANIZATION NAME AND ADDRESS: Naval Research Laboratory, Washington, D.C. 20375	10. PROGRAM ELEMENT, PROJECT, TASK AREA & WORK UNIT NUMBERS: NRL Problem R02-84.401, 63534N, S4629, 54629
11. CONTROLLING OFFICE NAME AND ADDRESS	12. REPORT DATE: March 10, 1975
	13. NUMBER OF PAGES: 43
14. MONITORING AGENCY NAME & ADDRESS *(if different from Controlling Office)*: Department of the Navy, Naval Ship Systems Command, Washington, D.C. 20362	15. SECURITY CLASS. *(of this report)*: Unclassified
	15a. DECLASSIFICATION/DOWNGRADING SCHEDULE

16. DISTRIBUTION STATEMENT *(of this Report)*

Approved for public release; distribution unlimited.

17. DISTRIBUTION STATEMENT *(of the abstract entered in Block 20, if different from Report)*

18. SUPPLEMENTARY NOTES

19. KEY WORDS *(Continue on reverse side if necessary and identify by block number)*

Beam steering
Circular arc arrays
Conformal arrays
Parabolic arc arrays
Phase control method
Radiation patterns

20. ABSTRACT *(Continue on reverse side if necessary and identify by block number)*

One of the most important problems to be overcome in implementing conformal arrays is controlling the element phases for beam steering. A simplified approximate technique for controlling steering phases of conformal arrays on a general surface was developed. The technique is to divide the array into several subarrays and to judiciously locate the elements on the curved surface so that the conventional row – column phase setting can be used in each subarray. Because of the approximate nature of the technique, some phase errors are introduced. However, for a given array size and shape of the conformal surface, the number (arrays

(Conti...d)

DD FORM 1 JAN 73 1473 EDITION OF 1 NOV 65 IS OBSOLETE
S/N 0102-014-6601

SECURITY CLASSIFICATION OF THIS PAGE *(When Data Entered)*

20.

can be chosen such that phase errors are within a specified limit. Analytical and computed results are presented for the techniques application to arrays on circular and parabolic curves. The results show that in many practical cases the approximate technique can be used with negligible degradation in performance.

CONTENTS

INTRODUCTION 1

PHASE CONTROL OF CONFORMAL ARRAYS . . . 1

SIMPLIFIED PHASE–CONTROL TECHNIQUE . . . 4

APPLICATION OF THE SIMPLIFIED TECHNIQUE . . 6

Conformal Arrays on a Circular Arc 6
Conformal Arrays on a Parabolic Arc 26

CONCLUSIONS 38

REFERENCES 38

APPENDIX A – Determination of Subarray Element Coordinates 39

A SIMPLIFIED TECHNIQUE FOR PHASE CONTROL OF CONFORMAL ARRAYS

INTRODUCTION

Conformal-array antennas offer many advantages over conventional planar arrays or reflector antennas. However, they are more difficult to design and implement. One of the most important problems is controlling the element phases for beam steering. Theoretically, it is possible to compute the phase distribution necessary for each element to point the beam in a required direction, but if the required hardware or software are difficult and expensive to implement, then this distribution and theory have no significance. The conformal arrays investigated in the past have generally had simple shapes, such as the cylindrical and conical arrays. The techniques developed to control these arrays depend on the properties of their particular shapes. In this report, a simplified approximate technique is described for use in controlling the steering phases of conformal arrays on a general surface. The technique is to divide the conformal array into several subarrays. By judiciously locating the elements on the curved surface, the conventional row-and-column phase setting can be used within each subarray, although each subarray requires an additional phase shift to compensate for the phase difference caused by its position on the curved surface. However, this correction is much simpler than that required for a conventional conformal array in which each element requires this compensation. Because of the approximate nature of the technique, some phase errors are introduced. However, for a given array size and shape of the conformal surface, the number of subarrays can be chosen such that the phase errors are within a specified limit. Analytical and computed results (phase errors, relative gain, and radiation patterns) are obtained for the arrays on circular and parabolic curves using the technique described here. The results are compared with those of the exact techniques, and they show that in many practical cases the approximate technique described here, which simplifies the hardware and software necessary for the phase control of the conformal arrays on a general surface, can be used with negligible degradation in array performance.

PHASE CONTROL OF CONFORMAL ARRAYS

The complexity of controlling the element phases to scan the beam of a conformal phased array increases greatly as the geometry of the conformal surface becomes more complex. The following examples in two dimensions illustrate the point.

The simplest case is a uniformly spaced linear array like that shown in Fig. 1. The phase needed at element n to scan the beam to an angle φ_o from broadside is given by

$$\beta_n = Knd \sin\varphi_o \tag{1}$$

Note: Manuscript submitted December 26, 1974.

where

K = the free-space wave number

n = the element number

d = interelement spacing

φ_o = scan angle from broadside.

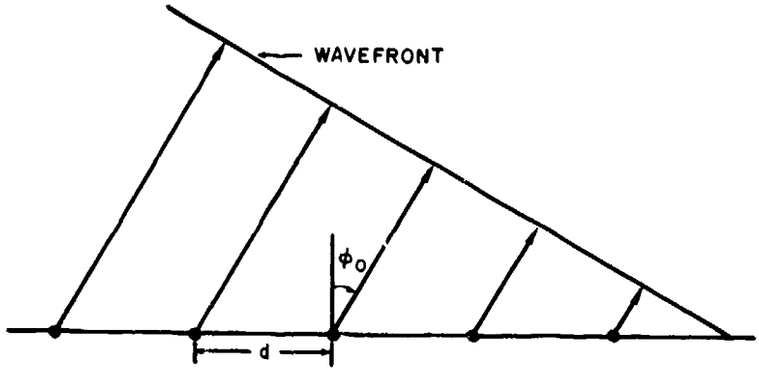

Fig. 1 — Geometry of a uniformly spaced linear array, scanned to an angle ϕ_o from broadside

Note, from Eq. (1), that the phase of each succeeding element can be obtained by adding $Kd \sin\varphi_o$ to the preceding element phase. Thus, this excitation may be implemented simply with a single adder at each element and a generator for $Kd \sin\varphi_o$.

The next level of complexity is a circular array with uniformly spaced elements. The array configuration is shown in Fig. 2. The phase needed at element n is given by

$$\beta_n = K\,R\,\cos\left[\varphi_o - (n-1)\frac{2\pi}{N}\right] \tag{2}$$

where

R = radius of curvature of the circular array

n = element number

φ_o = beam-pointing direction

N = total number of elements in the circular array

K = free-space wave number.

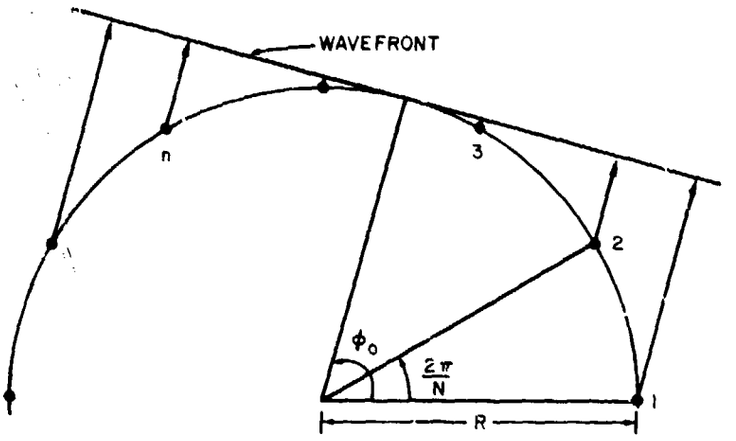

Fig. 2 — Geometry of a uniformly spaced circular array, scanned to an angle ϕ_0

From Eq. (2) it is clear that the phase needed at each element can be obtained only by calculating $\cos\left[\varphi_o - (n-1)\,2\pi/N\right]$ for each element. Thus, there are N times as many calculations as in the linear-array case.

Now, consider an array on a general two-dimensional curve, as shown in Fig. 3. Let the position of the element n be given by (x_n, y_n). The phase needed to scan the beam to an angle φ_o is given by

$$\beta_n = K\,(X_n \cos\varphi_o - Y_n \sin\varphi_o) \tag{3}$$

where

K = free-space wave number

φ_o = beam-pointing direction

(X_n, Y_n) = position of element n.

From Eq. (3) it is seen that the calculation of the phase needed at each element is more complicated for a general conformal array than for a circular array, since it involves the evaluating $X_n \cos\varphi_o$ and $Y_n \sin\varphi_o$ and adding them up for each element. The cost of the hardware and software to implement this configuration could make the system impractical.

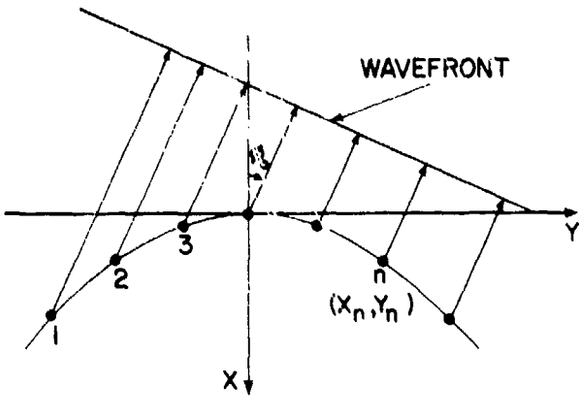

Fig. 3 — Geometry of a conformal array on a general surface, scanned to an angle ϕ_o

SIMPLIFIED PHASE-CONTROL TECHNIQUE

It has been shown [1] that for a limited scan angle and for large radius of curvature of conformal surface, the radiation pattern may be scanned by using the simple well-known technique of linear array phasing when the array elements are judiciously located on the conformal surface as discussed below.

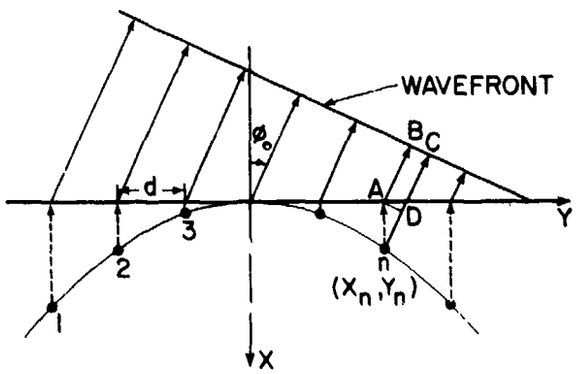

Fig. 4 — Geometry of a conformal array whose elements are projected onto a plane surface and scanned to an angle φ_o using linear array phasing

Consider a general two-dimensional conformal array, as shown in Fig. 4, with its elements phased in such a way that the wave emanating from the array is a plane wave traveling in a given direction φ_o. Approximately, this can be thought of as a projection of the elements on some plane surface, as shown in Fig. 4; linear array phasing is then

applied to the projected elements. If the elements are located on the conformal surface so that they have equal interelement spacing in the projected plane, we have an equivalent of a uniformly spaced linear array in the projected plane. Now, the beam may be scanned by using the simple well-known technique of the uniformly spaced linear array. What this approximation means is as follows: If the element n is located at (X_n, Y_n), the phase it needs to scan the beam to φ_o is approximated by

$$\overline{\beta_n} = K\,(X_n - Y_n \sin\varphi_o) \tag{4}$$

instead of the exact phase given by Eq. (3). The first term KX_n in Eq. (4) is a constant phase (not dependent on scan angle φ_o) that corresponds to the path length (shown as a dotted line in Fig. 4) between the actual and projected element positions. The second term $KY_n \sin\varphi_o$ corresponds to the linear array phasing.

From Eqs. (3) and (4) one can obtain the amount of phase error introduced by the approximate method in element n. This is given by

$$\epsilon_n = \overline{\beta_n} - \beta_n = KX_n\,(1 - \cos\varphi_o). \tag{5}$$

From Eq. (5) it may be noted that the phase error becomes zero when $\varphi_o = 0$. The phase error increases with an increase in φ_o or X_n. Therefore, if φ_o or X_n or both are small such that ϵ_n is not appreciable (say less than $\pi/4$), the approximate phasing can be used with negligible degradation in array performance. However, in many practical cases these conditions will not be met. In those cases it is still possible to use the linear array approximation if the conformal array is divided into several subarrays, as shown in Fig. 5, and the approximation technique is applied to individual subarrays. The effect of this is to decrease phase errors ϵ_n by decreasing X_n. Equations (3), (4), and (5) can be used with each subarray if X_n, Y_n, and φ_o are measured in subarray coordinates. In addition to the element phases, an additional phase (which depends on the scan angle) is required in each subarray to compensate for the phase difference caused by its position on the curved surface. However, this correction is much simpler than that required for a conventional conformal array in which each element requires this compensation. To obtain more insight into the approximate phasing technique and its usefulness, the next section is devoted to the application of the technique to conformal arrays on circular and parabolic curves.

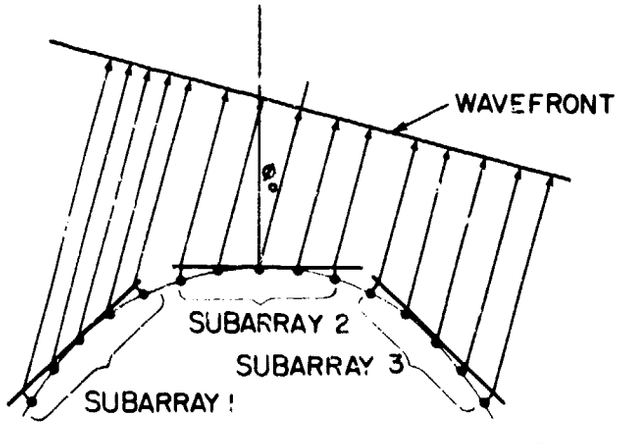

Fig. 5 — Geometry of a large conformal array divided into subarrays. Each subarray is scanned to obtain a beam at an angle ϕ_o using linear array phasing

APPLICATION OF THE SIMPLIFIED TECHNIQUE

The simplified technique for phase control of conformal arrays discussed in the previous section is quite general and could be used for arrays on any conformal surface. However, with no loss in generality, the technique will be applied here to conformal arrays on circular and parabolic curves, illustrating the usefulness and the limitations of the approximate technique.

Conformal Arrays on a Circular Arc

To reduce back lobes and high side lobes caused by the directivity of individual elements, usually only a part of the full circle is activated at any one time. Therefore, in what follows, it is assumed that the active part of the array is on a circular arc with an arc angle φ_A that is less than or equal to 180°. Let the array be divided into M equal subarrays, with φ_s being the subarray arc angle that is also equal to φ_A/M, as shown in Fig. 6. The subarray centers (or reference points) are assumed to be on the circular arc and can be shown to be at the angles given by

$$\varphi_m = \left(m - \frac{M}{2} - \frac{1}{2}\right)\varphi_s, \qquad m = 1, 2, \ldots, M \tag{6}$$

from the array broadside.

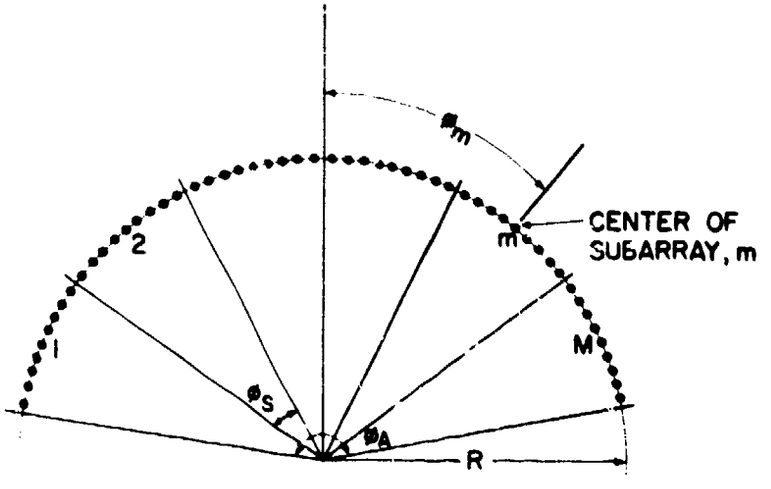

Fig. 6 — Geometry of a circular arc array divided into equal subarrays

To obtain some insight into the amount of element phase error introduced by the approximate phasing and how the phase errors depend on the radius of curvature R, the number of subarrays M, and the total array size, first consider a single subarray m as shown in Fig. 7. The subarray coordinates are represented by X_s and Y_s, with the

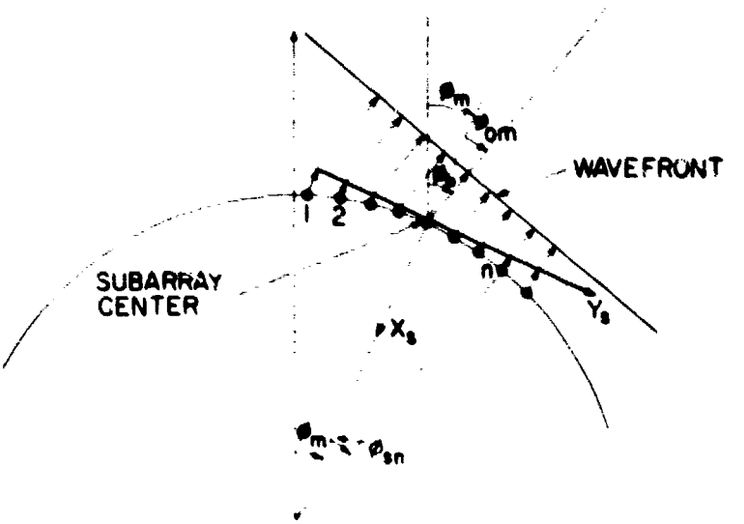

Fig. 7 — Geometry of subarray m scanned to an angle φ_{om} from its broadside direction

subarray center as the origin. The elements on the subarray are located so that when projected onto the Y_s axis they have equal interelement spacing D_{ys}, which is assumed to be known. If (Y_{sn}, X_{sn}) is the location of element n whose angular position from subarray broadside is given by ϕ_{sn}, then the following relations are satisfied:

$$\begin{aligned} Y_{sn} &= R \sin \varphi_{sn} \\ X_{sn} &= R\,(1 - \cos \varphi_{sn}). \end{aligned} \tag{7}$$

If the subarray broadside direction is φ_m with respect to full array reference coordinates, as shown in Fig. 7, then to scan the complete array to an angle φ_o means that the subarray m should be scanned by an angle $\varphi_{om} = \varphi_o - \varphi_m$ from its broadside. Therefore, the exact phase ψ_{omn} and the approximate phase $\overline{\psi}_{omn}$ needed at the element n of the subarray m to point the beam to an angle φ_o can be obtained from Eqs. (3) and (4) by substituting X_{sn} for X_n, Y_{sn} for Y_n, and φ_{om} for φ_o. They are given by

$$\psi_{omn} = KR\left[(1 - \cos\varphi_{sn})\cos\varphi_{om} - \sin\varphi_{sn}\sin\varphi_{om}\right] \tag{8}$$

and

$$\overline{\psi}_{omn} = KR\left[(1 - \cos\varphi_{sn}) - \sin\varphi_{sn}\sin\varphi_{om}\right]. \tag{9}$$

The phase error introduced by the approximate method in element n of the subarray m can be obtained by taking the difference between $\overline{\psi}_{omn}$ and ψ_{omn}. It is given by

$$\epsilon_{mn} = KR\,(1 - \cos\varphi_{sn})\,(1 - \cos\varphi_{om}). \tag{10}$$

The normalized phase error ϵ_{mn}/KR is plotted in Fig. 8 as a function of φ_{sn} with φ_{om} as a parameter. As can be noted from this figure, the normalized phase error increases very rapidly as φ_{sn} and φ_{om} are increased. It is instructive to note that no phase error is introduced in the element located at the center of the subarray, and the error increases as the element's angular position increases, the maximum error being introduced in the end elements of the subarray, whose angular positions are given by $\pm\varphi_{SN}$. Also, it may be noted that the element phase errors in the subarray are symmetrical about its center. What this means is that the beam-pointing direction is not affected by the phase errors, but there will be some decrease in array gain depending on the amount of phase errors. However, there may be some shift in the beam direction if the array elements have directive patterns. This will be discussed later.

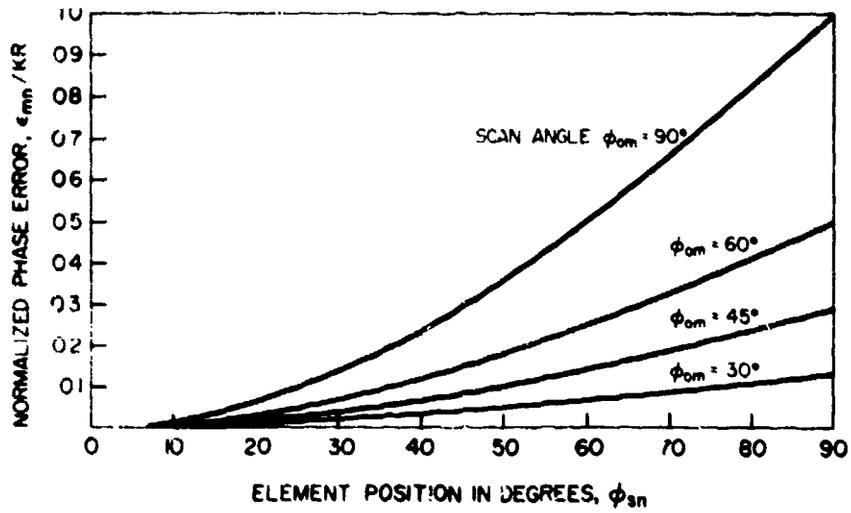

Fig. 8 — Phase errors in circular arc arrays when the linear array phasing method is used for beam scanning

For the circular array under consideration, the M subarrays are similar except for their angular positions φ_m with respect to the array broadside. Therefore, Eqs. (8), (9), and (10) can be applied to all the subarrays by using the correct value of φ_m. From Eq. (10) it may be noted that the phase error in any subarray depends not only on the element's angular position φ_{sn} but also on its scan angle φ_{om}. The maximum phase phase error occurs in the end elements of the subarray whose scan angle φ_{om} is maximum. In reference to the maximum value of φ_{om}, it is proper to say a few words on the way the circular array is scanned to cover 0° to 360°. It was mentioned earlier that only a part of the full circle is activated at any one time, and the active part occupies an arc angle φ_A that is divided into M subarrays with each subarray arc angle φ_s. These M subarrays are used to scan the beam over an angular range of

$-\varphi_s/2 \leqq \varphi_o \leqq \varphi_s/2$, using the approximate phasing technique discussed earlier. To cover other values of φ_o, an appropriate segment of the circle should be chosen as the active part of the array. For example, to cover the scanning range $\varphi_s/2 \leqq \varphi_o \leqq \varphi_s$, the subarray 1 is switched off, and the subarray M+1 is switched on. Note that the maximum value of $|\varphi_{om}| = |\varphi_o - \varphi_m|$ corresponds to the subarrays farthest from the center of the active part of the array. It can be shown very easily that

$$|\varphi_{om}|_{\max} = \frac{\varphi_A}{2}. \tag{11}$$

The maximum value of φ_{sn} corresponds to the end elements of each subarray and is equal to $(\varphi_s/2) = (\varphi_A/2M)$. Thus,

$$|\varphi_{sn}|_{\max} = \varphi_A/2M. \tag{12}$$

Substituting the maximum values for φ_{sn} and φ_{om} from Eqs. (11) and (12) into Eq. (10), one obtains the maximum element error when the approximate phasing technique is used. This is given by

$$\epsilon_{\max} = KR\left(1 - \cos\frac{\varphi_A}{2M}\right)\left(1 - \cos\frac{\varphi_A}{2}\right). \tag{13}$$

It should be clear that this maximum phase error is introduced only in the end elements of the subarrays that are farthest from the array center when the beam is scanned to $\pm\varphi_s/2$ from the array broadside. For the other elements in these subarrays and for all the elements in the other subarrays the phase errors are smaller than $\epsilon_{\max}$.

Several interesting results can be obtained by using Eq. (13). The first result is to find the maximum subarray size L_s (arc length $R\varphi_s$) that can be used for given values of R and φ_A such that the maximum phase error $\epsilon_{\max}$ will not exceed a specified value. Equation (13) can be rewritten as

$$\epsilon_{\max} = KR\left[1 - \cos\left(L_s/2R\right)\right]\quad\left[1 - \cos\left(\varphi_A/2\right)\right]. \tag{14}$$

Solving equation (14) for L_s gives

$$L_s = 4R\sin^{-1}\left\{\sqrt{\epsilon_{\max}/2\,KR\,\left[1 - \cos\left(\varphi_A/2\right)\right]}\right\}. \tag{15}$$

In antenna theory [2] and practice a phase error of $\pi/4$ (corresponding to a path length error of $\lambda/8$) is considered to be acceptable. Our results, given later in the report, prove this to be true. Substituting $\epsilon_{\max}/K = \lambda/8$ in Eq. (15) gives

$$L_s = 4R\sin^{-1}\left\{\frac{1}{4\sqrt{(R/\lambda)\,\left[1 - \cos\left(\varphi_A/2\right)\right]}}\right\}. \tag{16a}$$

If $(R/\lambda)\left[1-\cos(\varphi_A/2)\right] \gtrsim 1$, which is satisfied in many cases of interest, L_s can be approximated by

$$L_s \approx \sqrt{R\lambda/2} \;/\; \sin(\varphi_A/4). \tag{16b}$$

From Eq. (16b) note that the maximum subarray is proportional to the square root of the radius of curvature for a given array arc angle φ_A. As shown in Fig. 9, the subarray size L_s is plotted as a function of R with ϕ_A as a parameter, using Eq. (16b). If R and φ_A are known, the curves in Fig. 9 can be used to find the maximum subarray size that can be used to limit the maximum phase errors to 45° or less.

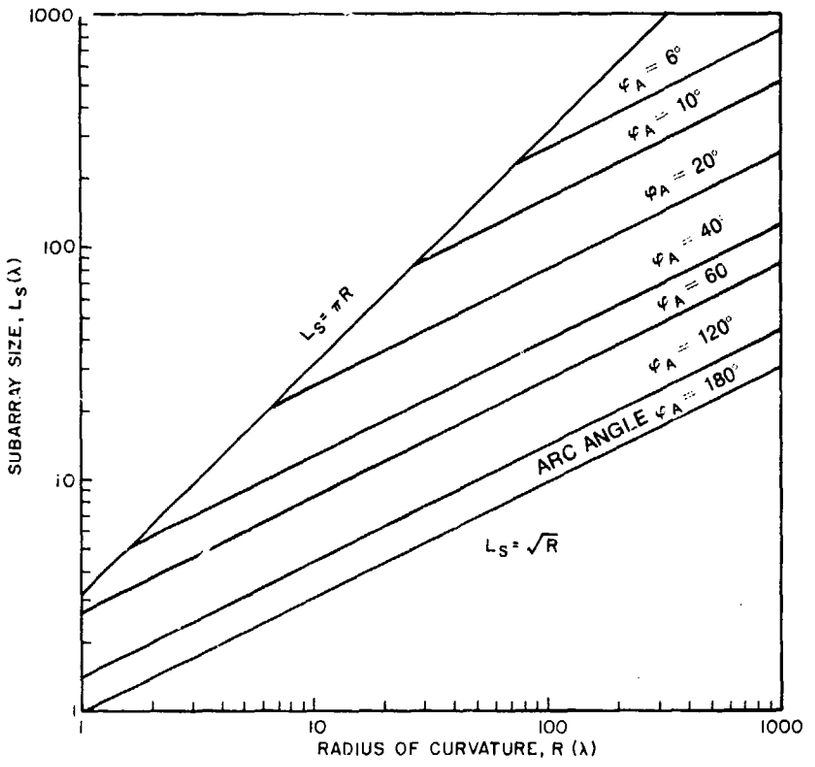

Fig. 9 — Maximum subarray size as a function of radius of curvature and arc angle for maximum path-length error of λ/8

Equation (13) can also be used to obtain the relation between the minimum number of subarrays needed as a function of R and the array size (specified by arc angle φ_A or arc length $L_A = R\varphi_A$) such that the maximum phase error ϵ_{max} will not exceed a specified value. Equation (13) can be rewritten as

$$\sin^2\left(\frac{\varphi_A}{4M}\right) = (\epsilon_{max}/2KR)/\left[1-\cos(\varphi_A/2)\right]. \tag{17}$$

First taking a square root and then the sine inverse on both sides of Eq. (17) readily shows that

$$M = \frac{\varphi_A}{4} \frac{1}{\sin^{-1}\left\{\sqrt{\epsilon_{max}/2KR\ [1 - \cos(\varphi_A/2)]}\right\}}. \tag{18}$$

For $(\epsilon_{max}/K) = \lambda/8$, F 4. (18) becomes

$$M = \frac{\varphi_A}{4} \frac{1}{\sin^{-1}\left\{1/4\sqrt{2R}\sin(\varphi_A/4)\right\}}. \tag{19a}$$

Using the same approximation as used in obtaining Eq. (16b), one obtains

$$M \approx \varphi_A \sqrt{2R} \sin(\varphi_A/4). \tag{19b}$$

Equations (19a) and (19b) are used to plot the number of subarrays M as a function of R with φ_A as a parameter. The number M is plotted in Fig. 10. As can be noted from this figure, the value of M needed increases with the increase in R for a given φ_A and increases with φ_A for a given value of R. These curves can be used to find the minimum number of subarrays into which the active part of the array is to be divided such that the maximum phase error ϵ_{max} will not exceed 45° for a given array size specified by R and φ_A.

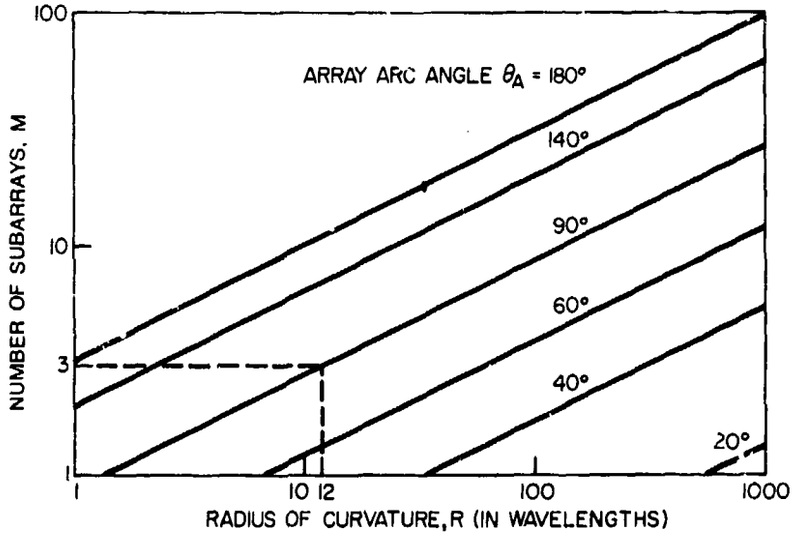

Fig. 10 — Number of subarrays as a function of radius of curvature and array arc angle for a maximum path-length error of $\lambda/8$

When the array size is specified by the arc length $L_A = R\varphi_A$ instead of arc angle φ_A, M can be expressed as a function of L_A and R by replacing φ_A by L_A/R in Eq. (19a) and (19b) as shown in Eqs. (20a) and (20b):

$$M = \frac{L_A}{4R} \frac{1}{\sin^{-1}\left\{1/4\sqrt{2R}\sin\left(L_A/4R\right)\right\}} \tag{20a}$$

$$M \approx \frac{L_A}{\sqrt{R}} \frac{\sqrt{2}}{} \sin\left(L_A/4R\right) . \tag{20b}$$

The number of subarrays M as a function of R with L_A as parameter is plotted in Fig. 11. From this figure it can be noted that the number of subarrays needed decreases with increase in R for a given value of L_A. This is intuitively obvious, because as R is increased, keeping L_A constant, the curved surface becomes more and more flat and coincides with a linear array as $R \to \infty$.

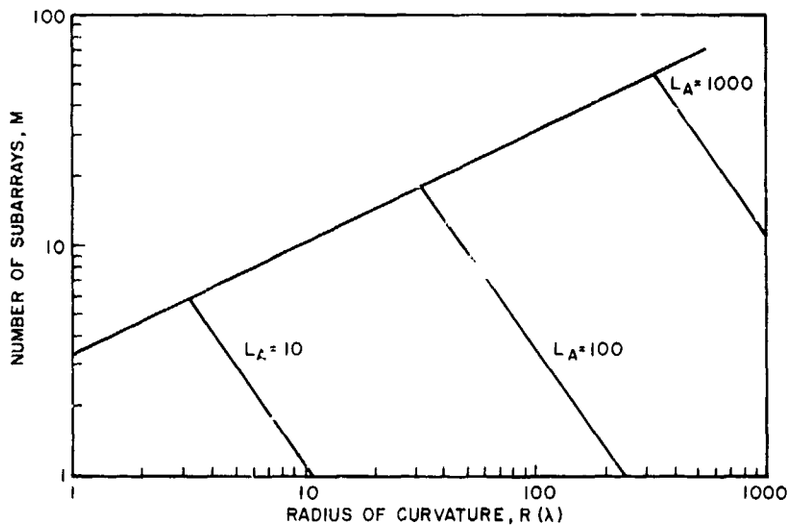

Fig. 11 — Number of subarrays as a function of radius of curvature and array arc length for a maximum path-length error of $\lambda/8$

So far the discussion has been concentrated on the element phase errors introduced by the approximate phasing technique and on how these phase errors are reduced by increasing the number of subarrays into which the conformal array is divided. Also, methods have been discussed for finding the minimum number of subarrays (or maximum subarray size), when the radius of curvature and the size of the conformal array are given, such that the maximum element phase error does not exceed a specified value. Now, it is of interest to formulate the expressions for radiation patterns using exact and

approximate phasing, so as to assess the effect of phase errors on the radiation patterns and the relative gains.

Equation (8) gives the expression for the correct element phases necessary in subarray m to scan the beam to an angle φ_o from the array broadside. The reference point of these phases is the subarray center. To add the contributions of all the subarrays, it is convenient if the reference point is moved to the center of the circle. Thus, if the center of the circle is referenced, the correct element phases are given by

$$\gamma_{omn} = \psi_{omn} - KR \cos \varphi_{om} . \tag{21}$$

Substituting the value of ψ_{omn} from Eq. (8) into Eq. (21), one obtains

$$\gamma_{omn} = -KR \cos (\varphi_o - \varphi_m - \varphi_{sn}) . \tag{22}$$

Since $\varphi_m + \varphi_{sn}$ represents the angular position of element n in subarray m, measured from the broadside direction of the circular array, the expression given in Eq. (22) coincides with the well-known result [3] of the circular array element phase necessary to scan the beam to an angle φ_o. If the nth element pattern in subarray m is given by $E_{mn}(\varphi)$, then the radiation pattern of subarray m is given by

$$F_m = \sum_{n=1}^{N} E_{mn} (\varphi) \, e^{j(\gamma_{mn} + \gamma_{omn})} \tag{23}$$

where

$$\gamma_{mn} = KR \cos (\varphi - \varphi_m - \varphi_{sn}) . \tag{24}$$

Since the reference point is the same for all the subarrays, the radiation pattern of an active circular arc array composed of M subarrays can be obtained by simply adding all the subarray patterns and is given by

$$F(\varphi) = \sum_{m=1}^{M} F_m = \sum_{m=1}^{M} \sum_{n=1}^{N} E_{mn} (\varphi) \, e^{jKR \left[\cos (\varphi - \varphi_m - \varphi_{sn}) - \cos (\varphi_o - \varphi_m - \varphi_{sn})\right]} . \tag{25}$$

If exactly the same procedure is used, the radiation pattern can be formulated when the approximate phasing is used by simply replacing ψ_{omn} with $\overline{\psi}_{omn}$ in Eq. (21) and following the same steps used in obtaining Eq. (25). If $\overline{F}(\varphi)$ represents the radiation pattern obtained by using approximate phasing, it is given by

$$\overline{F}(\varphi) = \sum_{m=1}^{M} \sum_{n=1}^{N} E_{mn} (\varphi) \, e^{jKR \left[\cos (\varphi - \varphi_m - \varphi_{sn}) - \cos\varphi_{sn} - \sin (\varphi_o - \varphi_m) \sin\varphi_{sn} + 1 - \cos(\varphi_o - \varphi_m)\right]} . \tag{26}$$

A computer program was developed to obtain the radiation patterns by using Eqs. (25) and (26). A circular arc array with an arc angle $\varphi_A = 90^\circ$ and a radius of curvature $R = 12\lambda$ is taken as an example. For this example, note from Fig. 10 that the number of subarrays $M = 3$, indicating that the array should be divided into at least three subarrays to use the approximate phasing method such that the maximum phase error will be less than 45° (path length error of $\lambda/8$). However, to show clearly the effectiveness of reducing the phase errors by increasing the number of subarrays, the computed results will be given when the array is divided into 1, 2, and then 3 subarrays. In all the cases considered, the element pattern is assumed to be a cosine function with the peak of its pattern directed along the surface normal, where the element is located. For the circular array under consideration, the element pattern maximum will be in the radial direction. Thus, the element pattern is given by

$$E_{mn}(\varphi) = \cos(\varphi - \varphi_m - \varphi_{sn}) . \tag{27}$$

The number of elements and the element locations are determined in the following manner. Knowing the arc angle of the subarray and the radius of curvature, the projection of the subarray on the Y_s axis (see Fig. 7) is given by $L_p = 2R \sin(\varphi_s/2) = 2R \sin(\varphi'_A/2M)$, where φ'_A is obtained from the relation $2R \sin(\varphi'_A/2) = 2R \sin(\varphi_A/2) + 0.5\lambda$. If L_p is known, the number of elements N can be chosen such that the interelement spacing $D_{ys} = L_p/N$ is around 0.5λ. This procedure allows the end elements to be located at a distance $D_{ys}/2$ from the subarray endpoints and eliminates the possibility of locating the end elements of neighboring subarrays on top of each other. Once D_{ys} is known, the nth element position Y_{sn} can be found. Then, from Eq. (7), the angular position φ_{sn} can be found.

For $M = 1$, $\varphi_A = 90^\circ$, and $R = 12\lambda$, the number of elements, N is 35, and the interelement spacing $D_{ys} = 0.499\lambda$. The computed radiation patterns are shown in Fig. 12a to 12g for several scan angles using correct and approximate phase steering. Note that as the scan angle is increased the radiation patterns obtained by the approximate phase steering deteriorate, and the beam-pointing direction deviates from that of the patterns obtained with the correct phase steering. The reason for these effects is that the maximum phase error is 45° at a 17.5° scan angle and increases rapidly with the increase in scan angle. These phase errors decrease if the array is divided into several subarrays.

For $M = 2$, $\varphi_A = 90^\circ$, and $R = 12\lambda$, the number of elements in each subarray is given by $N = 19$, and the projected interelement spacing $D_{ys} = 0.5\lambda$. The total number of elements in the two subarrays is 38. For $M = 3$, $\varphi_A = 90^\circ$, and $R = 12\lambda$, the number of elements in each subarray is given by $N = 13$, and the projected interelement spacing is given by $D_{ys} = 0.495\lambda$. The total number of elements in the three subarrays is given by 39. Note that the number of elements needed is increased slightly with M because the total projected aperture increases with M. For M large, the projected aperture approaches the value $R\varphi_A$. The radiation patterns for the cases of $M = 2$ and 3 are shown in Figs. 13a-13f and 14a-14f, respectively. From these figures it may be noted that, when M is increased to three, the radiation patterns obtained by approximate phase steering are quite close to those obtained by correct phase steering even for scan angles as large as 60°. The decrease in phase errors and the corresponding improvement in array performance as the number of subarrays M is increased from one to three can be seen more

clearly from the gain loss curves shown in Fig. 15. In the actual implementation, the active part of the array is scanned to only $\pm\varphi_s/2$ (φ_s = the subarray arc angle) and the proper subarrays are switched on and off to cover the scanning range of 0° to 360°. When this switching and scanning of the subarrays is used, the loss in gain of the conformal array due to approximate phase steering is as shown in Fig. 16 for M = 1, 2, and 3. As may be seen clearly, the array performance is improved considerably as M is increased from 1 to 3.

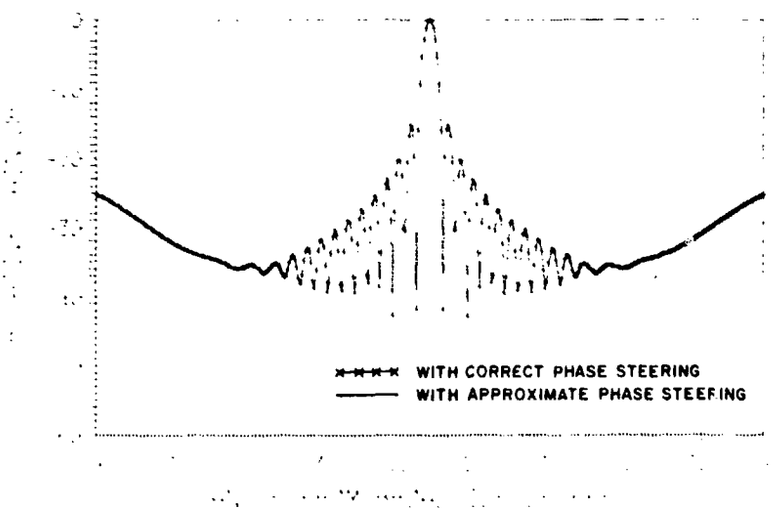

Fig. 12a — Broadside radiation patterns of a circular arc array, arc angle ϕ_A = 90°, and radius of curvature R = 12λ

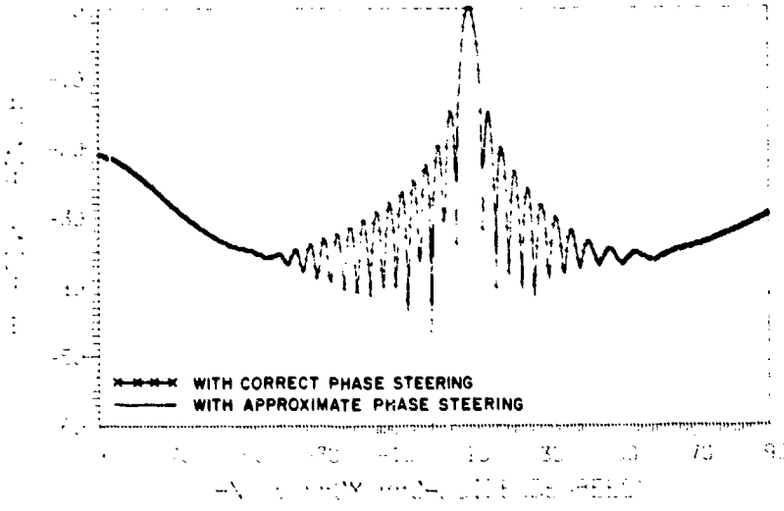

Fig. 12b — Radiation patterns of a circular arc array scanned to 10°, arc angle ϕ_A = 90°, and radius of curvature R = 12λ

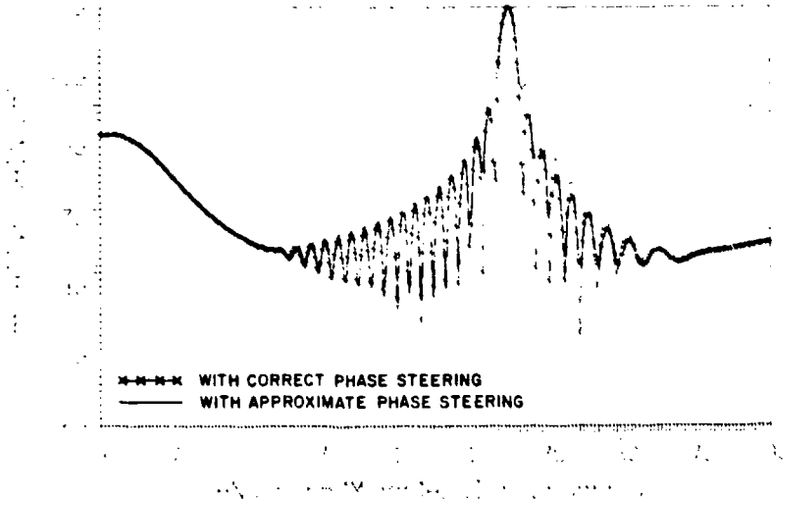

Fig. 12c — Radiation patterns of a circular arc array scanned to 20°, arc angle ϕ_A = 90°, and radius of curvature R = 12λ

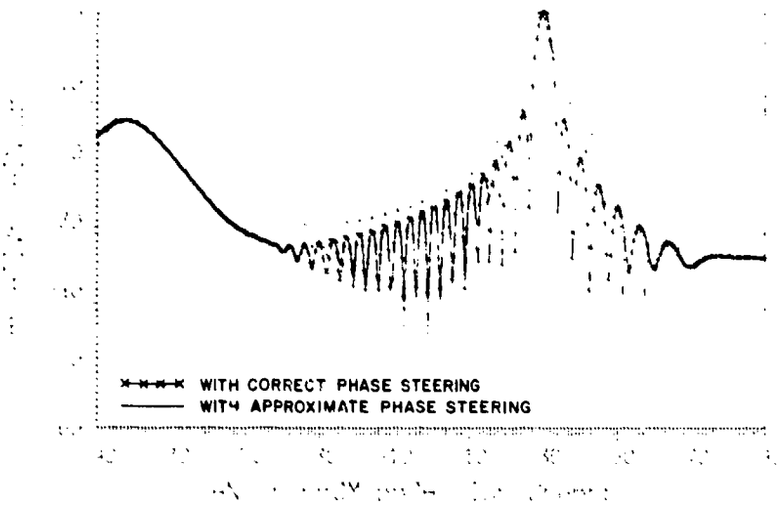

Fig. 12d — Radiation patterns of a circular arc array scanned to 30°, arc angle ϕ_A = 90°, and radius of curvature R = 12λ

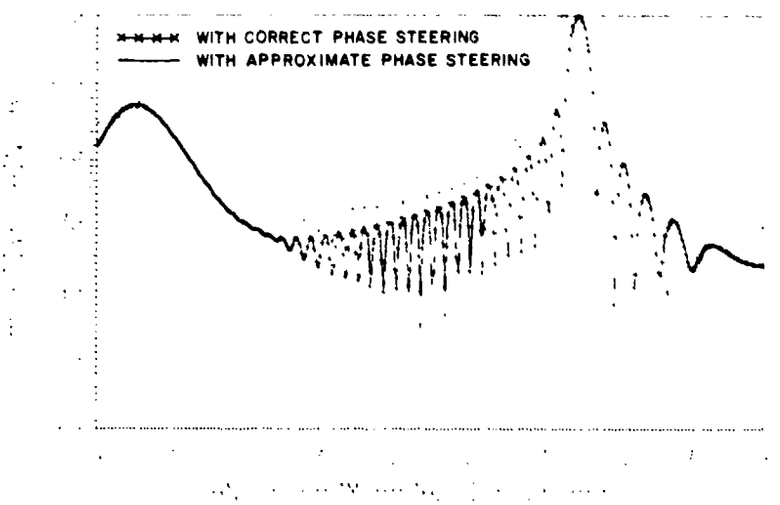

Fig. 12e — Radiation patterns of a circular arc array scanned to 40°, arc angle ϕ_A = 90°, and radius of curvature R = 12λ

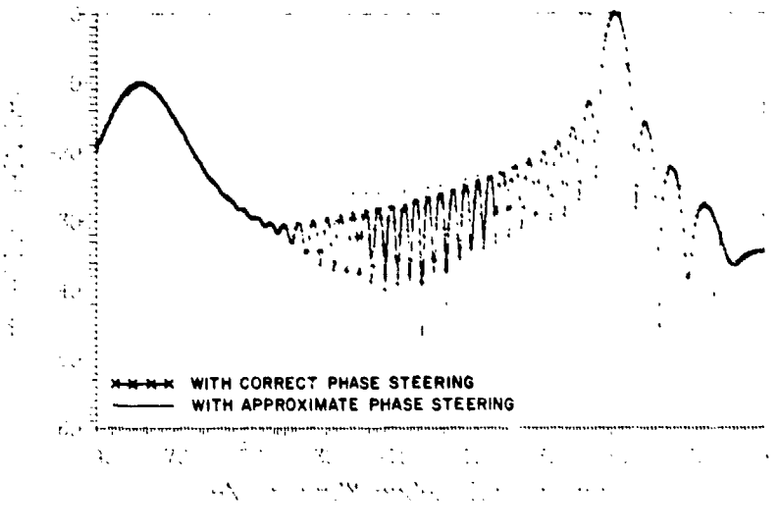

Fig. 12f — Radiation patterns of a circular arc array scanned to 50°, arc angle ϕ_A = 90°, and radius of curvature R = 12λ

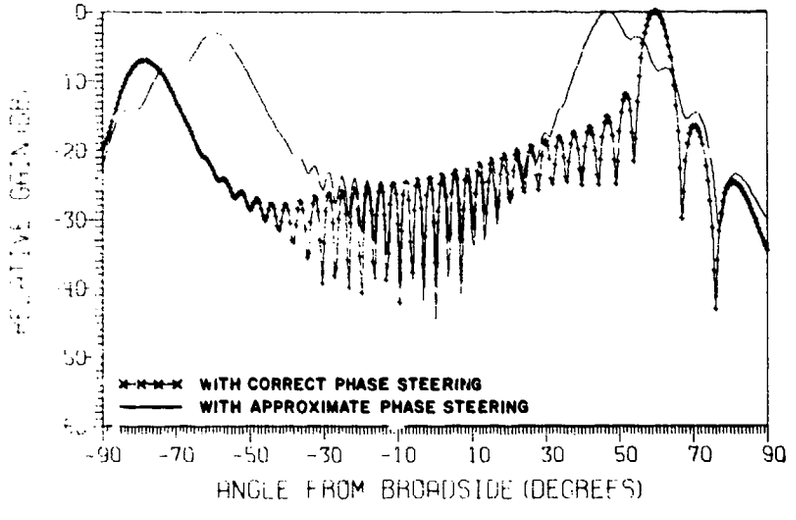

Fig. 12g — Radiation patterns of a circular arc array scanned to 60°, arc angle ϕ_A = 90°, and radius of curvature R = 12λ

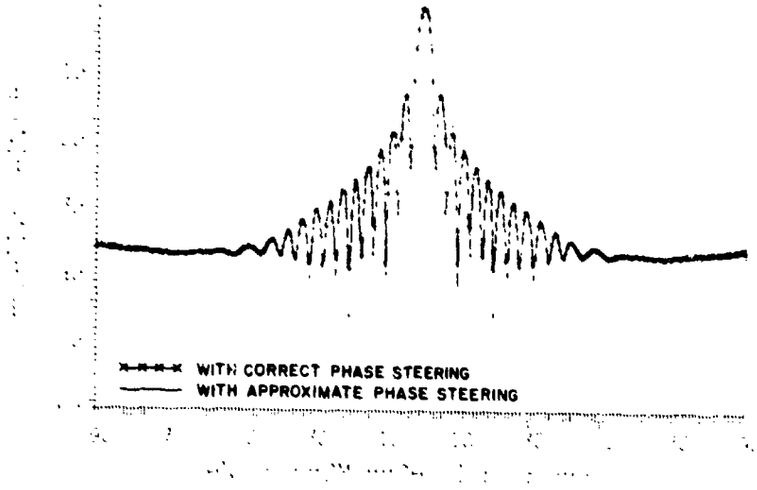

Fig. 13a — Broadside radiations patterns of a circular arc array divided into two subarrays, arc angle $\phi_A = 90°$, and radius of curvature $R = 12\lambda$

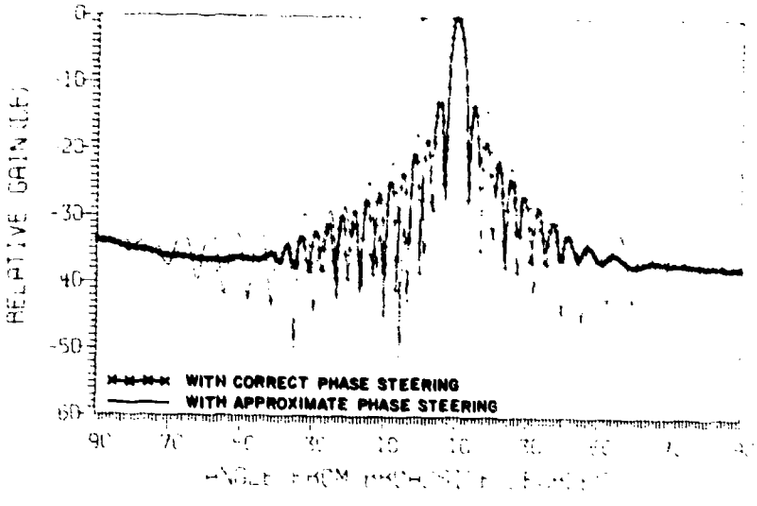

Fig. 13b — Radiation patterns of a circular arc array divided into two subarrays and scanned to 10°, arc angle $\phi_A = 90$, and radius of curvature $R = 12\lambda$

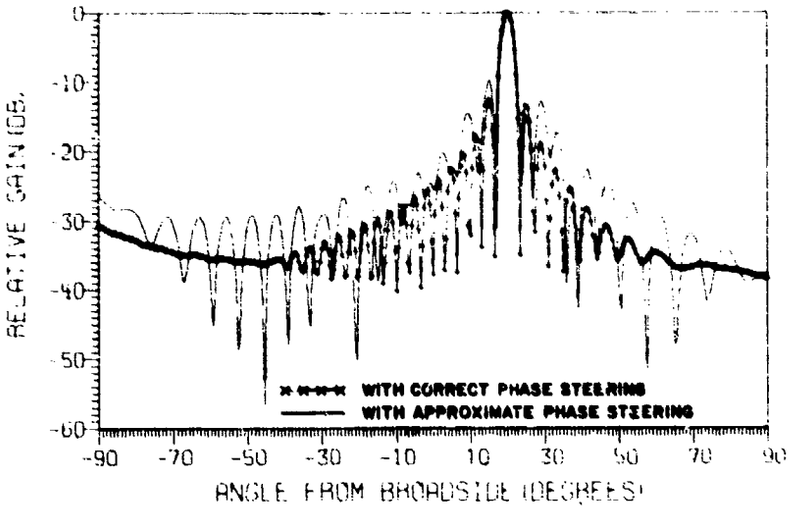

Fig. 13c — Radiation patterns of a circular arc array divided into two subarrays and scanned to 20°, arc angle ϕ_A = 90°, and radius of curvature $R = 12\lambda$

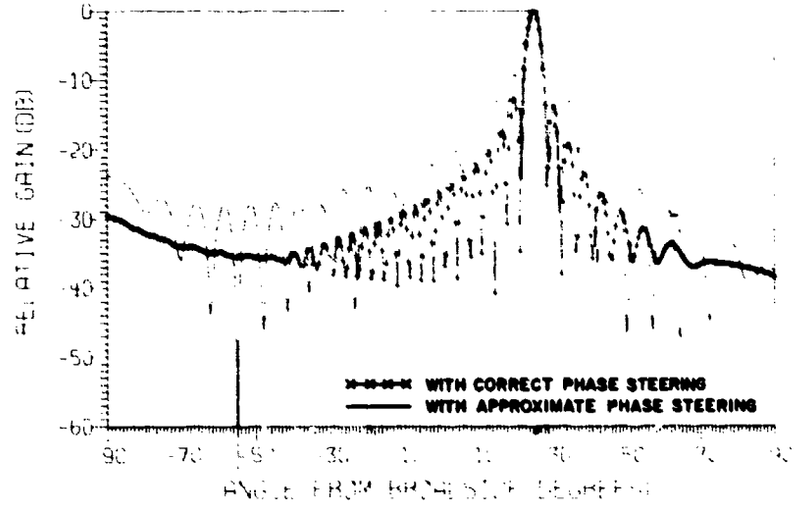

Fig. 13d — Radiation patterns of a circular arc array divided into two subarrays and scanned to 25°, arc angle ϕ_A = 90°, and radius of curvature $R = 12\lambda$

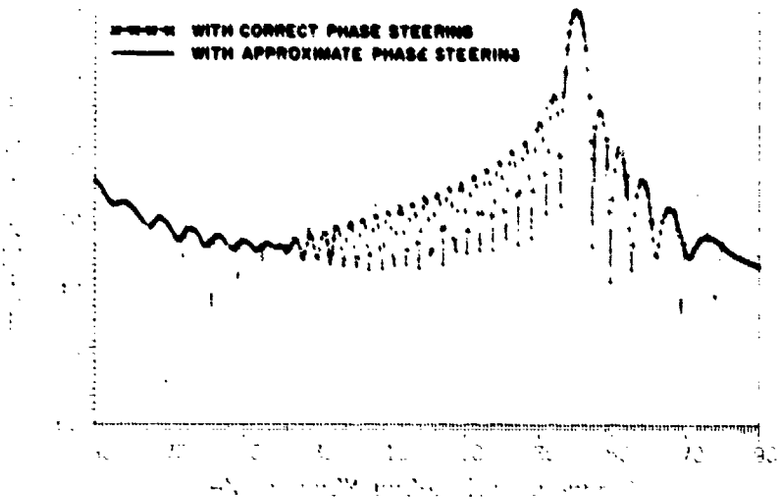

Fig. 13e — Radiation patterns of a circular arc array divided into two subarrays and scanned to 40°, arc angle ϕ_A = 90°, and radius of curvature R = 12λ

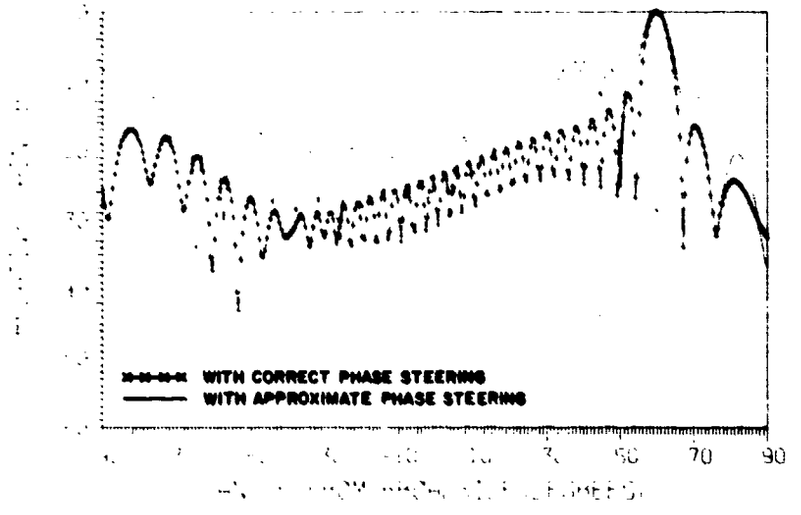

Fig. 13f — Radiation patterns of a circular arc array divided into two subarrays and scanned to 60°, arc angle ϕ_A = 90°, and radius of curvature R = 12λ

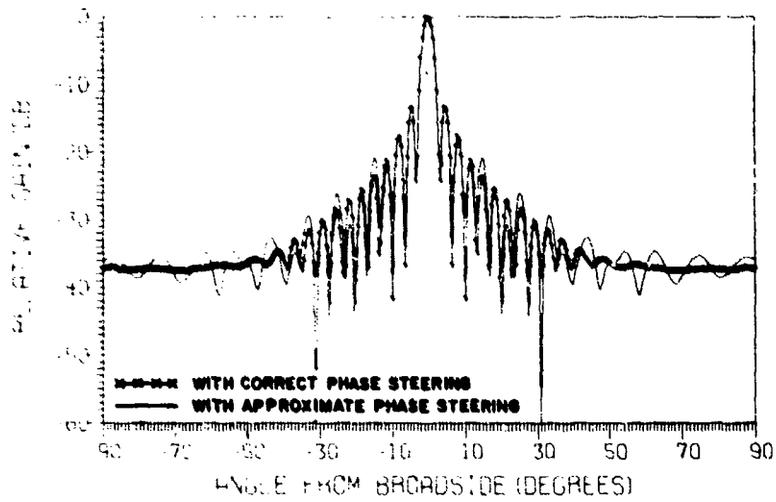

Fig. 14a — Broadside radiation patterns of a circular arc array divided into three subarrays, arc angle $\phi_A = 90°$, and radius of curvature $R = 12\lambda$

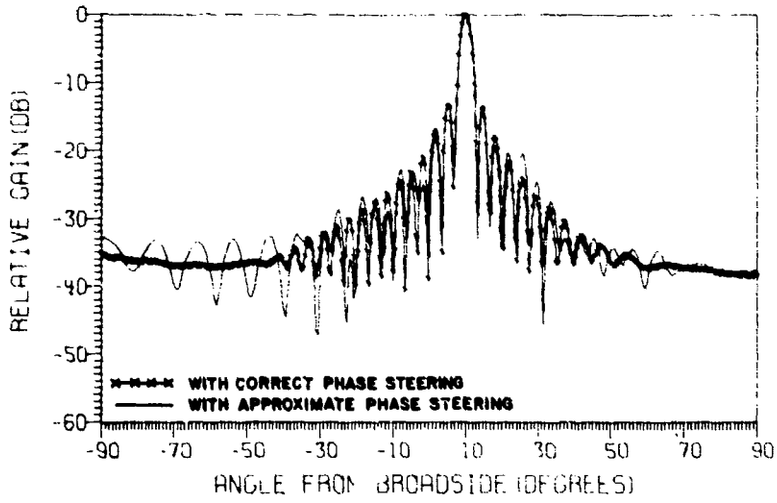

Fig. 14b — Radiation patterns of a circular arc array divided into three subarrays and scanned to 10°, arc angle $\phi_A = 90°$, and radius of curvature $R = 12\lambda$

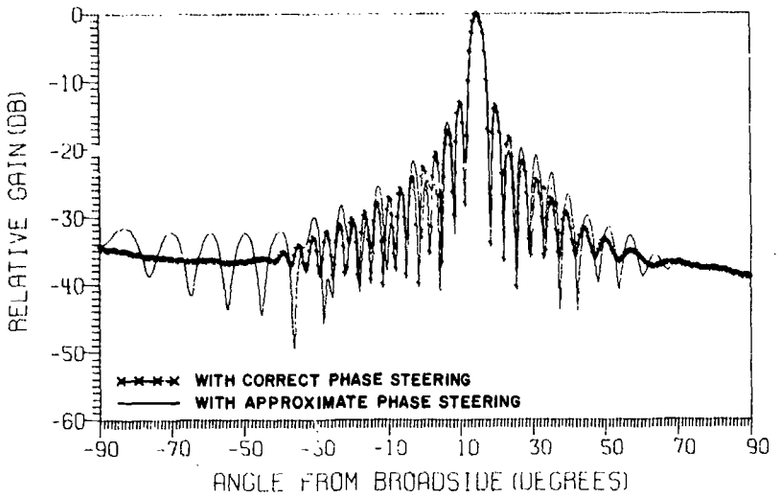

Fig. 14c — Radiation patterns of a circular arc array divided into three subarrays and scanned to 15°, arc angle ϕ_A = 90°, and radius of curvature R = 12λ

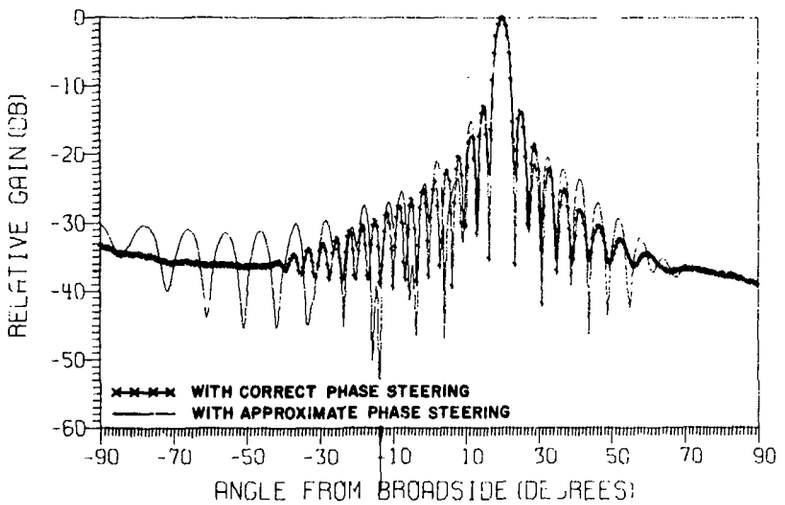

Fig. 14d — Radiation patterns of a circular arc array divided into three subarrays and scanned to 20°, arc angle ϕ_A = 90°, and radius of curvature R = 12λ

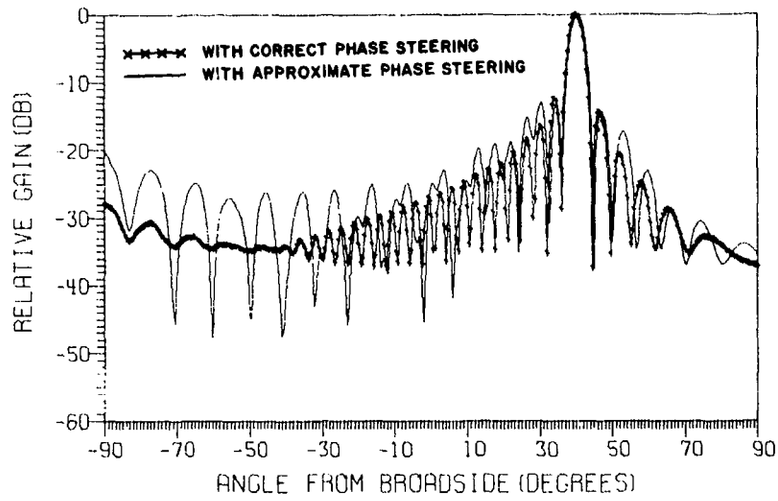

Fig. 14e — Radiation patterns of a circular arc array divided into three subarrays and scanned to 40°, arc angle ϕ_A = 90°, and radius of curvature R = 12λ

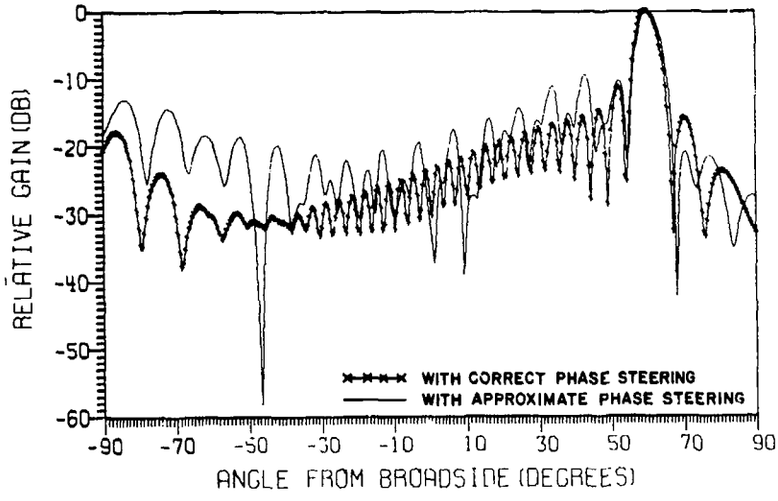

Fig. 14f — Radiation patterns of a circular arc array divided into three subarrays and scanned to 60°, arc angle ϕ_A = 90°, and radius of curvature R = 12λ

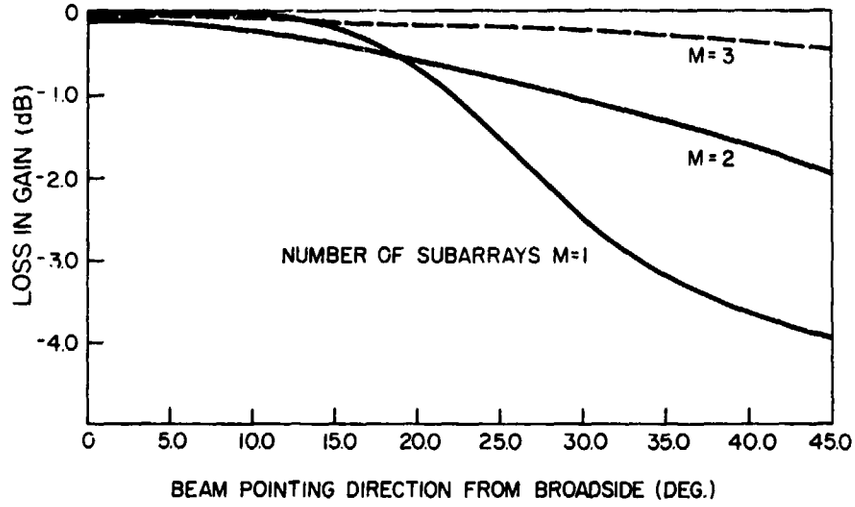

Fig. 15 — Loss in gain in a circular arc array due to phase errors introduced by simplified phase steering when the array is divided into M subarrays; arc angle ϕ_A = 90° and radius of curvature R = 12λ

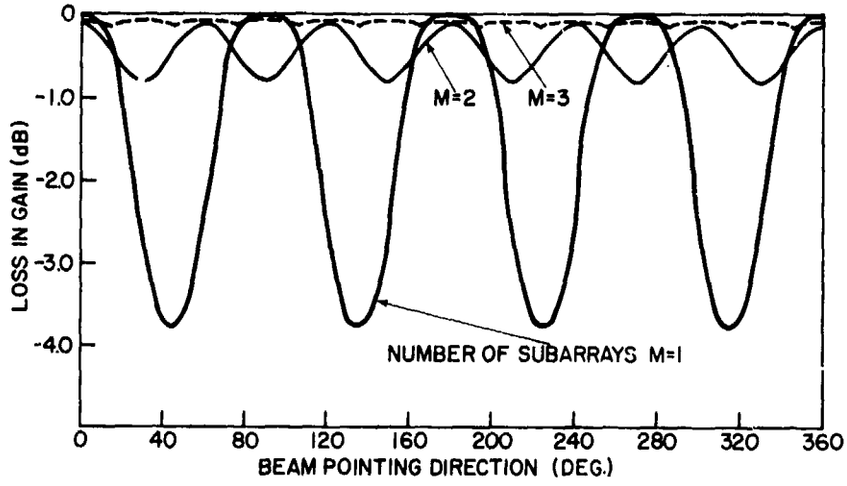

Fig. 16 — Loss in gain in a circular array due to phase errors introduced by simplified phase steering along with subarray switching to cover 360° scanning range; active arc angle ϕ_A = 90° and radius of curvature R = 12λ

Conformal Arrays on a Parabolic Arc

Conformal arrays on a parabolic arc are considered as a second example in applying simplified phase control. The array under consideration is shown in Fig. 17. The parabolic curve is defined by the equation

$$Y^2 = 4fX \tag{28}$$

where f is the focal length of the parabola.

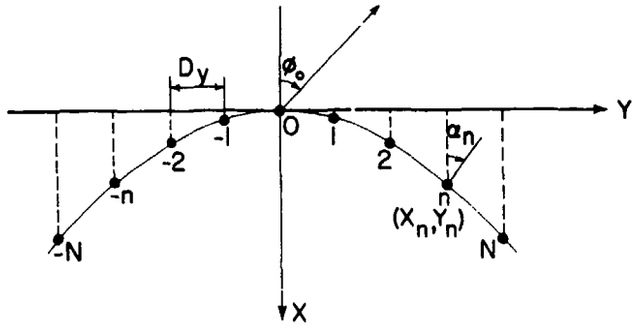

Fig. 17 — Geometry of a conformal array on a parabolic curve

Even though the principle of applying the simplified phasing technique to a parabolic arc array is simple and straightforward, the general analytical treatment given to a circular array that is divided into M subarrays cannot be extended to the parabolic arc array, since the circular symmetry no longer exists. Therefore, the parabolic arc array is treated separately when it is divided into one or two subarrays, respectively.

Figure 17 is applicable when the parabolic arc is considered as one subarray. If the element locations are given by (X_n, Y_n) on the parabolic arc, then the correct and approximate element phases needed to scan the beam to an angle φ_o from broadside are given by Eqs. (3) and (4). If $E_n(\varphi)$ is the nth element pattern, the array patterns $F(\varphi)$ and $\bar{F}(\varphi)$ obtained by using correct and approximate phasing, respectively, are given by

$$F(\varphi) = \sum_{n=-N}^{N} E_n(\varphi)\, e^{jK\left[X_n(\cos\varphi-\cos\varphi_o)-Y_n(\sin\varphi-\sin\varphi_o)\right]} \tag{29}$$

$$\bar{F}(\varphi) = \sum_{n=-N}^{N} E_n(\varphi)\, e^{jK\left[X_n(\cos\varphi-1)-Y_n(\sin\varphi-\sin\varphi)\right]}. \tag{30}$$

In Eqs. (29) and (30) it is assumed that there is an odd number of elements in the array, given by $2N + 1$. Similar equations can be obtained if there is an even number of elements in the array. Now, the problem is to find Y_n, X_n, and $E_n(\varphi)$ for the parabolic array under consideration. Y_n can be looked at as the projected element location on the Y axis. Therefore, the Y_n values are chosen such that the projected interelement spacing is a constant (say D_y). In other words, $|Y_n - Y_{n-1}| = D_y$. By substituting Y_n for Y in Eq. (28), one can obtain the value of X_n. Therefore,

$$Y_n = nD_y$$

and

$$X_n = Y_n^2/4f = n^2 D_y^2/4f \ . \tag{31}$$

As in the case of the circular array, we assume that the element pattern is a cosine function with its peak value directed normal to the conformal surface, where the element is located. For the parabolic arc the element pattern becomes

$$E_n(\varphi) = \cos(\varphi - \alpha_n) \tag{32}$$

where

$$\alpha_n = \tan^{-1}(Y_n/2f) = \tan^{-1}(nD_y/2f).$$

Knowing the array parameters D_y, N, and f, one can find Y_n, X_n, and $E_n(\varphi)$ using Eqs. (31) and (32) and substitute them in Eqs. (29) and (30) to find the radiation patterns. In addition, if the values of X_n are known, Eq. (5) can be used to estimate the element phase errors introduced by the simplified technique. If the maximum phase error exceeds a specified value, the array must be divided into subarrays before applying the simplified technique. The analytical treatment of dividing the parabolic array into several subarrays becomes very complicated and will not be undertaken. However, dividing the array into two subarrays will be formulated to show the effectiveness of subdividing the arrays.

Figure 18 shows the parabolic array divided into two subarrays. The projected aperture of the array on the Y axis is assumed known and is given by $2Y_A$. The array coordinates are given by X and Y. A coordinate system for one of the subarray coordinates is given by X_s and Y_s, as shown in Fig. 18. It can be seen from this figure that the subarray origin is at (X', Y') in the X, Y coordinate system, with $Y' = Y_A/2$ and $X' = Y' \tan\alpha$, where α is the angle between the broadside directions of the parabolic array and subarray, as shown if Fig. 18. It is given by $\tan\alpha = Y'/2f$. The projected aperture of the subarray on the Y_s axis is given by $Y_A/\cos\alpha$. If N_s is the number of elements in the subarray, then the elements are located on the subarray so that they have equal interelement spacing, given by $D_s = (Y_A/\cos\alpha)/N_s$. The reason for dividing by N_s rather than $N_s - 1$ is to locate the end elements at $D_s/2$ from the subarray endpoints rather than at the endpoints, as shown in Fig. 18. This procedure eliminates the possibility of locating the end elements of the two subarrays on top of one another. If

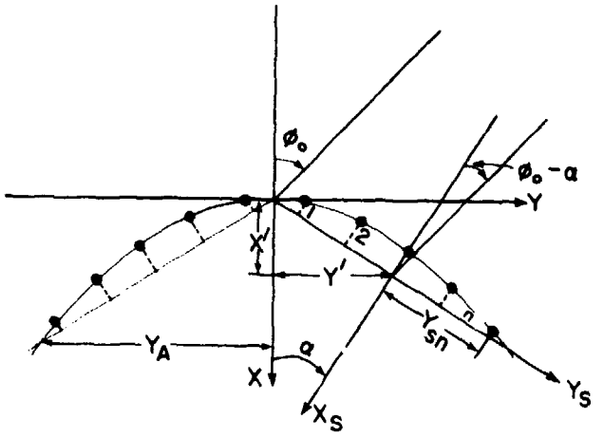

Fig. 18 — Geometry of a conformal array on a parabolic curve, divided into two subarrays

D_s and N_s are known, it is fairly straightforward to determine Y_{sn}, the Y_s coordinate of the nth element in the subarray. If Y_{sn} is known, the X_s coordinate of the nth element X_{sn} can be found (see Appendix A) and is given by

$$X_{sn} = \frac{Y_{sn}}{\tan\alpha} + \frac{Y_A}{2\sin^3\alpha}\left(1 - \sqrt{1 + \sin^4\alpha - \frac{4Y_{sn}}{Y_A}\cos\alpha\sin^2\alpha}\right). \tag{33}$$

If the subarray element locations (Y_{sn}, X_{sn}) are known, the required phases to steer the beam to an angle φ_o from array broadside (angle $\varphi_o - \alpha$ from subarray broadside) can be obtained from Eqs. (3) and (4) by substituting X_{sn} for X_n, Y_{sn} for Y_n, and $\varphi_{o1} = \varphi_o - \alpha$ for φ_o. Therefore, the correct and approximate patterns of subarray 1 with its origin as the reference point are given by

$$E_{s1} = \sum_{n=1}^{N_s} E_{n1}(\varphi)\, e^{jK\left[X_{sn}(\cos\varphi - \cos\varphi_{o1}) - Y_{sn}(\sin\varphi - \sin\varphi_{o1})\right]} \tag{34}$$

and

$$\vec{E}_{s1} = \sum_{n=1}^{N_s} E_{n1}(\varphi)\, e^{jK\left[X_{sn}(\cos\varphi - 1) - Y_{sn}(\sin\varphi - \sin\varphi_{o1})\right]}. \tag{35}$$

Where, E_{n1} is the pattern of the nth element in subarray 1 and is given by

$$E_{n1}(\varphi) = \cos(\varphi - \alpha_n), \tag{36}$$

where

$$\alpha_n = \tan^{-1}(Y_n/2f)$$
$$Y_n = Y' + Y_{sn}\cos\alpha - X_{sn}\sin\alpha. \tag{37}$$

Note that subarray 2 is the mirror image of subarray 1 with respect to the X axis. It is not difficult to show that the correct and approximate patterns of subarray 2 with its origin as the reference point are given by

$$E_{s2} = \sum_{n=1}^{N_s} E_{n2}(\varphi)\, e^{jK\left[X_{sn}(\cos\varphi - \cos\varphi_{o2}) + Y_{sn}(\sin\varphi - \sin\varphi_{o2})\right]} \tag{38}$$

$$\overline{E}_{s2} = \sum_{n=1}^{N_s} E_{n2}(\varphi)\, e^{jK\left[X_{sn}(\cos\varphi - 1) + Y_{sn}(\sin\varphi - \sin\varphi_{o2})\right]} \tag{39}$$

where

$$E_{n2} = \cos(\varphi + \alpha_n) \tag{40}$$

$$\varphi_{02} = \varphi_0 + \alpha \tag{41}$$

and α_n is given by Eq. (37).

To obtain the parabolic array pattern in the X, Y coordinate system, we add the subarray patterns vectorially, with the midpoint of the two subarray centers as the reference point. These patterns are given by

$$F(\varphi) = E_{s1}\, e^{jKY'(\sin\varphi - \sin\varphi_o)} + E_{s2}\, e^{-jKY'(\sin\varphi - \sin\varphi_o)} \tag{42}$$

and

$$\overline{F}(\varphi) = \overline{E}_{s1}\, e^{jKY'(\sin\varphi - \sin\varphi_o)} + \overline{E}_{s2}\, e^{-jKY'(\sin\varphi - \sin\varphi_o)} \tag{43}$$

where $F(\varphi)$ and $\overline{F}(\varphi)$ are the correct and approximate parabolic array patterns when the array is divided into two subarrays.

A parabolic arc array with $f = 4\lambda$ and the Y-axis projected aperture of 9λ is considered as a numerical example. If the array is approximated by a single subarray, the projected interelement spacing $D_y = 0.5\lambda$, the number of elements in the array $2N + 1 = 19$, and the element locations are defined by Eq. (31). Correct and approximate radiation patterns are computed using Eqs. (29) and (30) and are shown in Figs. 19a to 19g. From these figures it may be noted that the patterns obtained by approximate phase steering deteriorate as the scan angle is increased above 30°, and the beam-pointing direction deviates more and more from those patterns obtained by using correct steering phase as the scan angle is increased. The reason for this is that for this example the maximum phase error is 45° if the scan angle is 25.7°, and it increases as the scan angle increases. It will be shown later that there is a corresponding loss in array gain. Therefore, if the array needs to be scanned to more than 30° from broadside, the array should be divided into subarrays. The radiation patterns are computed from Eqs. (42) and (43) when the array is divided into two subarrays and are shown in Figs. 20a-20g for several scan angles. As can be seen from these figures, the array patterns with approximate phase steering coincide very closely with those obtained by using correct phase steering. The decrease in phase errors and the corresponding improvement in array performance when the array is divided into two subarrays can be seen more clearly from the gain loss curves shown in Fig. 21.

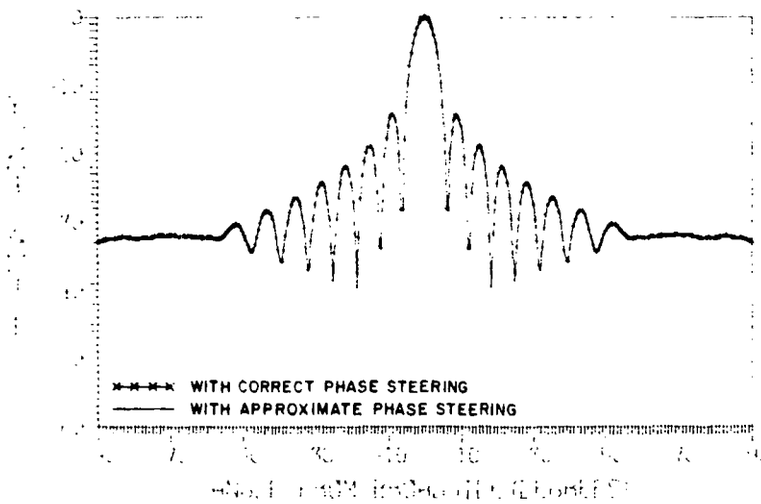

Fig. 19a — Broadside radiation patterns of a 19-element array on a parabolic arc: projected aperture on Y axis, 9.0λ; focal length of the parabola, $f = 4\lambda$

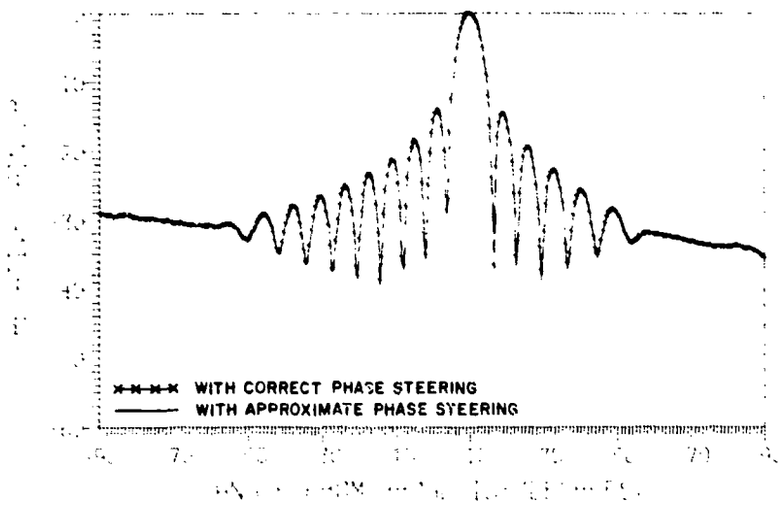

Fig. 19b — Radiation pattern of a 19-element array on a parabolic arc, scanned to 10° from broadside: projected aperture on Y axis, 9.0λ; focal length of the parabola, $f = 4\lambda$

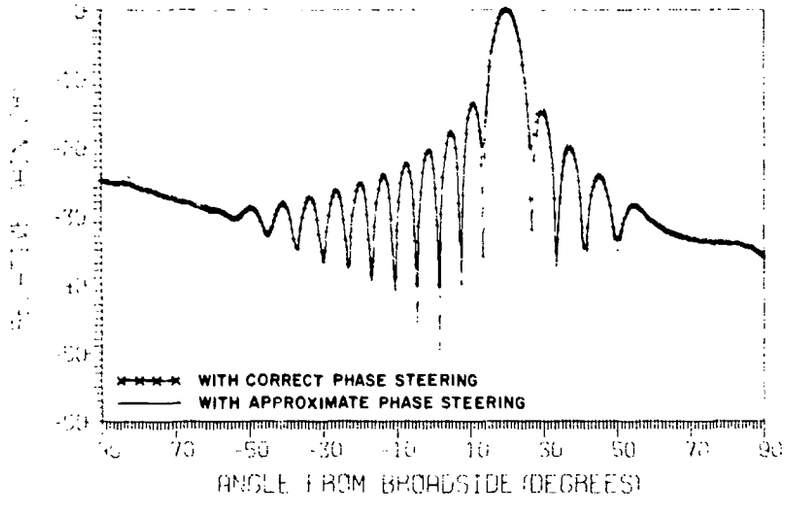

Fig. 19c — Radiation patterns of a 19-element array on a parabolic arc, scanned to 20° from broadside: projected aperture on Y axis, 9.0λ; focal length of the parabola, $f = 4\lambda$

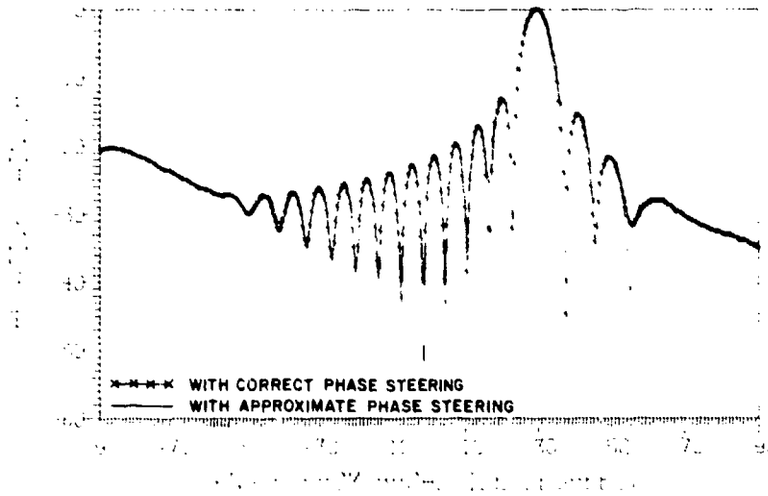

Fig. 19d — Radiation patterns of a 19-element array on a parabolic arc, scanned to 30° from broadside: projected aperture on Y axis, 9.0λ; focal length of the parabola, $f = 4\lambda$

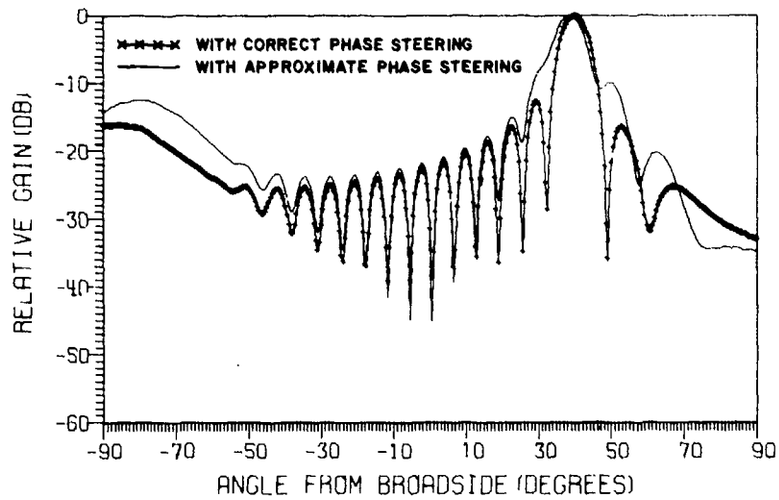

Fig. 19e — Radiation patterns of a 19-element array on a parabolic arc, scanned to 40° from broadside: projected aperture on Y axis, 9.0λ; focal length of the parabola, $f = 4\lambda$

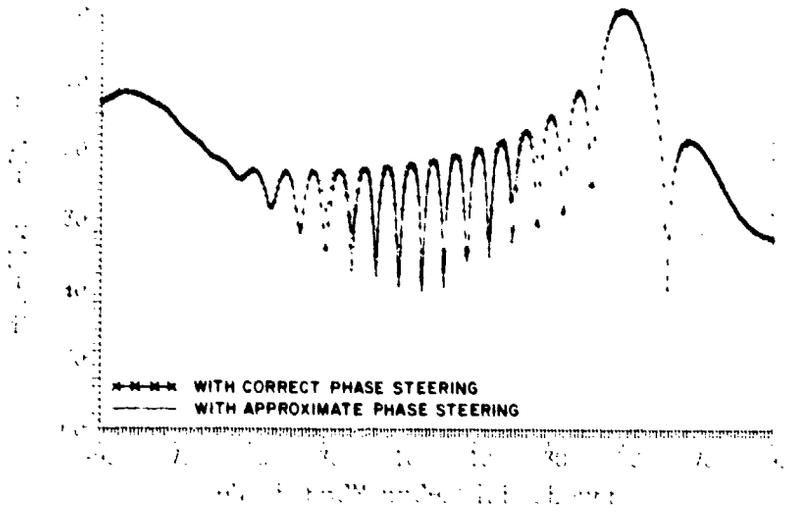

Fig. 19f — Radiation patterns of a 19-element array on a parabolic arc, scanned to 50° from broadside: projected aperture on Y axis, 9.0λ; focal length of the parabola, $f = 4\lambda$

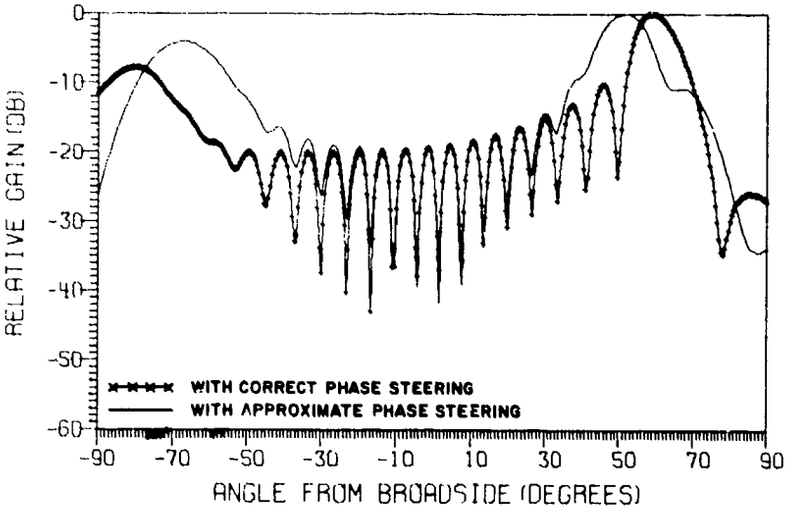

Fig. 19g — Radiation patterns of a 19-element array on a parabolic arc, scanned to 60° from broadside: projected aperture on Y axis, 9.0λ; focal length of the parabola, $f = 4\lambda$

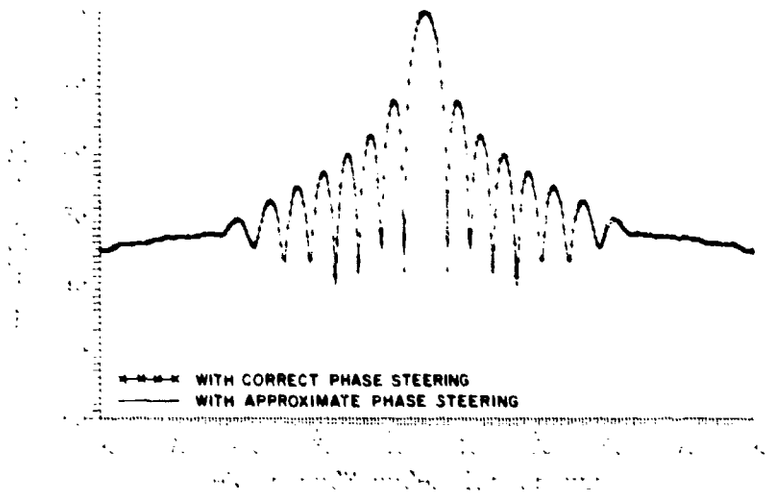

Fig. 20a — Broadside radiation patterns of an array on a parabolic arc, divided into two subarrays: 10 elements in each subarray; projected aperture on Y axis, 9.0λ; focal length of the parabola, $f = 4\lambda$

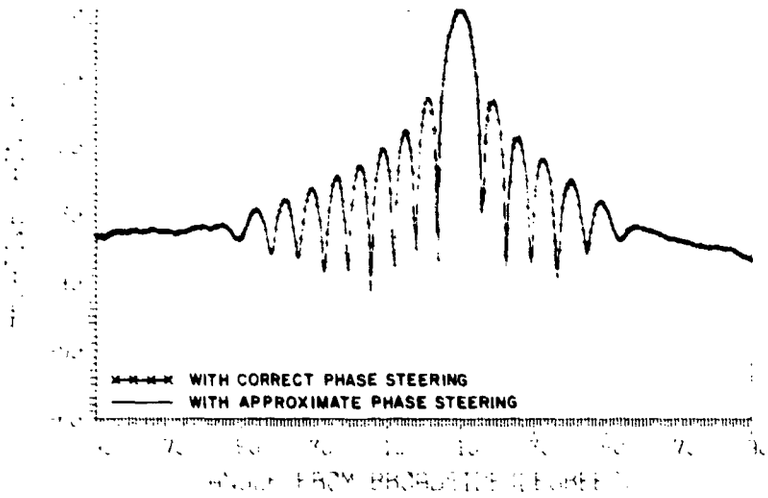

Fig. 20b — Radiation patterns of an array on a parabolic arc, divided into two subarrays and scanned to 10°: 10 elements in each subarray; projected aperture on Y axis, 9.0λ; focal length of the parabola, $f = 4\lambda$

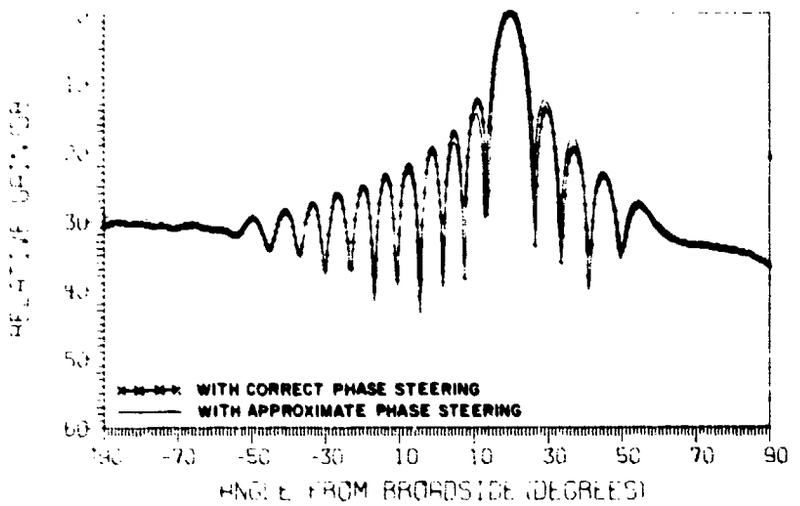

Fig. 20c — Radiation patterns of an array on a parabolic arc, divided into two subarrays and scanned to 20°: 10 elements in each subarray; projected aperture on Y axis, 9.0λ; focal length of the parabola, f = 4λ

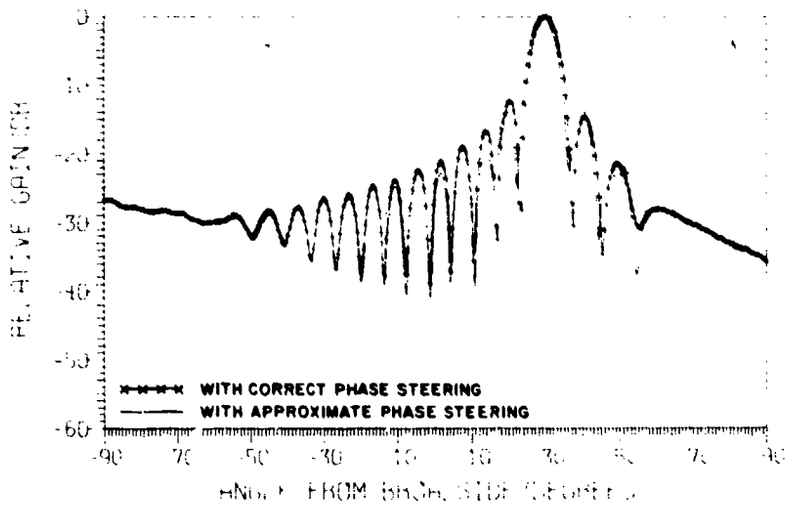

Fig. 20d — Radiation patterns of an array on a parabolic arc, divided into two subarrays and scanned to 30°: 10 elements in each subarray; projected aperture on Y axis, 9.0λ; focal length of the parabola, f = 4λ

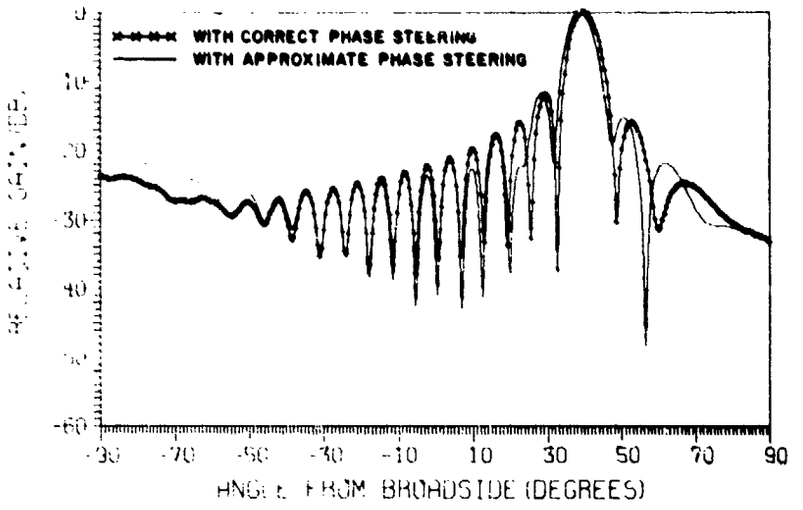

Fig. 20e — Radiation patterns of an array on a parabolic arc, divided into two subarrays and scanned to 40°: 10 elements in each subarray; projected aperture on *Y* axis, 9.0λ; focal length of the parabola, $f = 4\lambda$

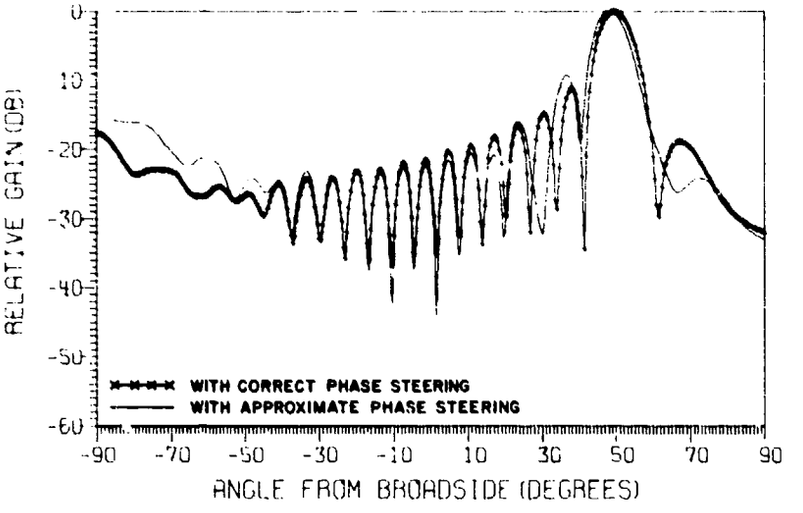

Fig. 20f — Radiation patterns of an array on a parabolic arc, divided into two subarrays and scanned to 50°: 10 elements in each subarray; projected aperture on *Y* axis, 9.0λ; focal length of the parabola, $f = 4\lambda$

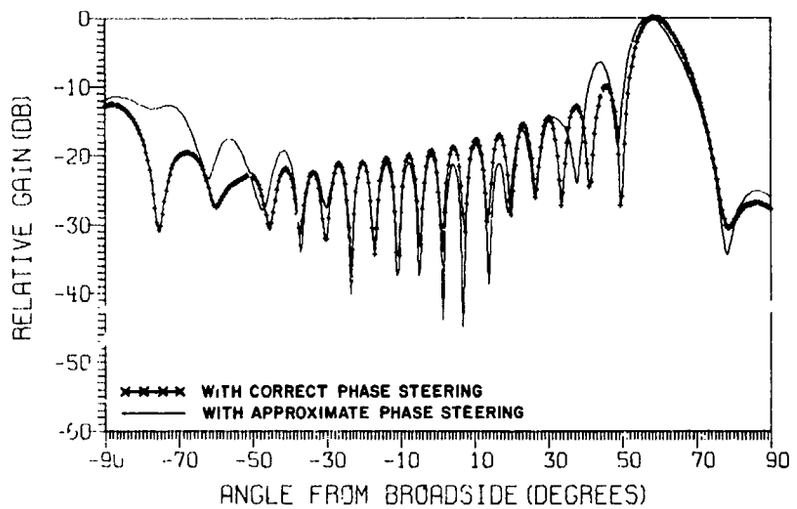

Fig. 20g — Radiation patterns of an array on a parabolic arc, divided into two subarrays and scanned to 60°: 10 elements in each subarray: projected aperture on Y axis, 9.0λ; focal length of the parabola, $f = 4\lambda$

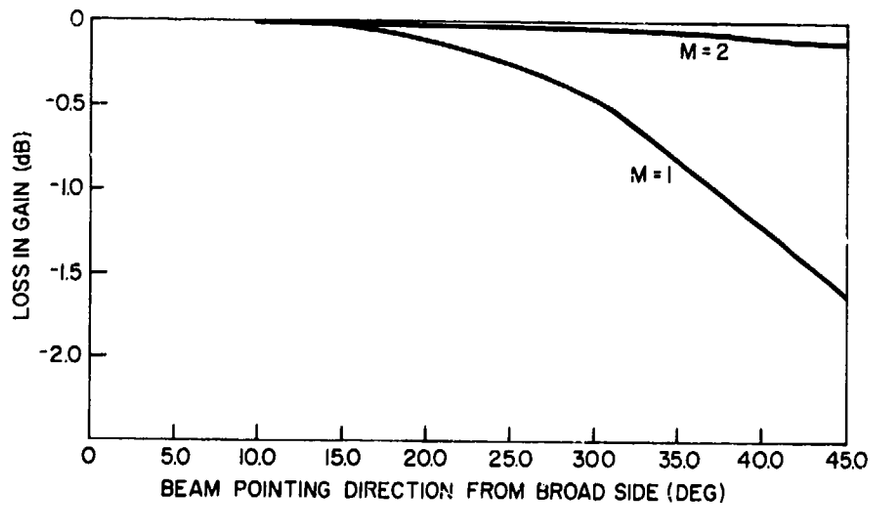

Fig. 21 — Loss in gain in a parabolic arc array due to phase errors introduced by simplified phase steering when the array is divided into M subarrays: projected aperture on Y axis, 9.0λ; focal length of the parabola, $f = 4\lambda$

CONCLUSIONS

In this report, we have presented an approximate technique that simplifies the hardware and software necessary for phase control of conformal arrays on a general surface. Analytical and computed results are presented for the tecnique as applied to arrays on circular and parabolic curves. The results show that in many practical cases the approximate technique can be used with negligible degradation in array performance.

REFERENCES

1. G.V. Vaughn, "A Technique for Control of Conformal Arrays," Proc. Array Antenna Conf., Report TD 155, Vol. 1, Part 2, Naval Electronics Laboratory Center, San Diego, Calif., Feb. 22-24, 1972.

2. S. Silver, editor, *Microwave Antenna Theory and Design*, Dover Publications, New York, 1965, p. 431.

3. M.T. Ma, *Theory and Application of Antenna Arrays*, Wiley Interscience, New York, 1974, pp. 191-193.

Appendix A
DETERMINATION OF SUBARRAY ELEMENT COORDINATES

In Fig. A1, note that to obtain an equation of the parabolic curve in the subarray coordinate system it is first necessary to translate the origin to (X', Y') and then rotate the coordinates by an angle α. These coordinate transformations result in the relations

$$X = X_s \cos\alpha - Y_s \sin\alpha + X' \tag{A1}$$

and

$$Y = X_s \sin\alpha + Y_s - Y' \ . \tag{A2}$$

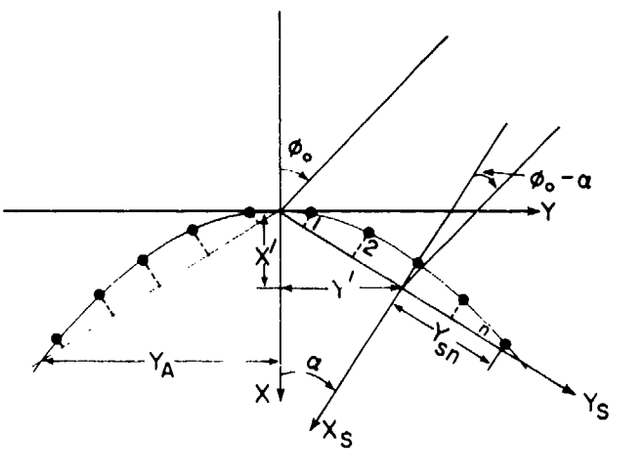

Fig. A1 — Geometry of a conformal array on a parabolic curve, divided into two subarrays

Substituting these relations for X and Y in the equation defining the curve ($Y^2 = 4fx$) and rearranging the terms, we obtain the following equation for the parabola:

$$X_s^2 + X_s\left(\frac{2Y_s}{\tan\alpha} - \frac{4F}{\tan^2\alpha \cos^3\alpha}\right) + Y_s^2 \cos^2\alpha - \frac{Y_A^2}{4 \sin^2\alpha} = 0 \ . \tag{A3}$$

If Y_{sn} is the Y_s coordinate of the nth element in the subarray, the X_s coordinate X_{sn} of this element can be obtained by solving Eq. (A3) for X_s by substituting $Y_s = Y_{sn}$. Only one of the two solutions is the correct value, given by (Eq. (33) in text)

$$X_{sn} = \frac{Y_{sn}}{\tan\alpha} + \frac{Y_A}{2\sin^3\alpha}\left(1 - \sqrt{1 + \sin^4\alpha - \frac{4\,Y_{sn}}{Y_A}\cos\alpha\sin^2\alpha}\right). \qquad \text{(A4)}$$